Evaluation of Anthropogenic Emissions and Ozone Pollution in the North China Plain: Insights from the Air Chemistry Research in Asia (ARIAs) Campaign

Hao He[1], Xinrong Ren[1,2,3], Sarah E. Benish[1], Zhanqing Li[1,4,5], Fei Wang[5,6], Yuying Wang[5], Timothy P. Canty[1], Xiaobo Dong[7], Feng Lv[7], Yongtao Hu[8], Tong Zhu[9], and Russell R. Dickerson,[1,4]

[1]Department of Atmospheric and Oceanic Science, University of Maryland, College Park, MD 20742, USA

[2]Air Resources Laboratory, National Oceanic and Atmospheric Administration, College Park, MD 20742, USA

[3]Cooperative Institute for Climate and Satellites, University of Maryland, College Park, Maryland, USA

[4]Earth System Science Interdisciplinary Center, University of Maryland, College Park, MD 20740, USA

[5]College of Global Change and Earth System Science, Beijing Normal University, Beijing, 100875, China

[6]Key Laboratory for Cloud Physics, Chinese Academy of Meteorological Sciences, Beijing, 100081, China

[7]Weather Modification Office of Hebei Province, Shijiazhuang, 050021, China

[8]School of Civil & Environmental Engineering, Georgia Institute of Technology, Atlanta, GA 30332, USA

[9]College of Environmental Sciences and Engineering, Peking University, Beijing 100871, China

Keywords: Ozone Production Sensitivity, Airborne Measurements, OMI, CMAQ

Corresponding to Dr. Hao He (haohe@umd.edu)

Abstract

To study the air pollution in the North China Plain (NCP), the Air Chemistry Research in Asia (ARIAs) campaign conducted airborne measurements of air pollutants including O_3, CO, NO and NO_2 in spring 2016. High concentrations of pollutants, with maximum values >100 ppbv of O_3, >500 ppbv of CO, and >10 ppbv of NO_2, were observed throughout the boundary layer during the campaign. CMAQ simulations with the 2010 EDGAR emissions can capture the basic spatial and temporal variations of ozone and its major precursors such as CO, NO_x and VOCs, but significantly underestimate their concentrations. Observed emission enhancements of CO and NO_x with respect to CO_2 suggest the existence of combustion with high emissions such as biomass burning in the NCP. The comparison with emission factors calculated from the 2010 EDGAR emission inventory indicates that EDGAR overestimated the contribution of combustion with high emissions ~~has been overestimated~~. Differences between CMAQ simulations with 2010 emissions and satellite observations in 2016 can reflect the change in anthropogenic emissions. NO_x emissions decreased in megacities such as Beijing and Shanghai confirming the effectiveness of recent control measures in China, while in other cities and rural areas NO_x emissions slightly increased, e.g., CMAQ predicts only ~~80~~81% of NO_x observed in the aircraft campaign area. CMAQ also underestimates HCHO (a proxy of VOCs, by ~20%) and CO (by ~60%) over the NCP, suggesting adjustments of the 2010 EDGAR emissions are needed to improve the model performance. HCHO/NO_2 column ratios derived from OMI measurements and CMAQ simulations show that VOC-sensitive chemistry dominates the ozone photochemical production in eastern China, suggesting the importance of tightening regulations on VOCs emissions. ~~We~~ After ~~adjusted~~ adjusting EDGAR emissions based on satellite observations, we conducted sensitivity experiments of CMAQ~~,~~ and achieved better model performance in simulating ~~ozone~~column contents of air pollutants. ~~, b~~But CMAQ still underestimated~~imation still exists~~ air pollutant concentrations as compared with surface and aircraft observations. Because of the VOC-sensitive environment in ozone chemistry over the NCP, this study qualitatively suggested the underestimation of anthropogenic emissions could be important for CMAQ simulations while future study and regulations should focus on VOCs emissions with the continuous controls on NO_x emissions in China.

1. Introduction

With rapid economic growth in the past three decades, the consumption of energy in China increased dramatically (Zhang and Cheng, 2009; Guan et al., 2018; Shan et al., 2018). Fossil fuels dominate total energy consumption, with coal still accounting for more than 50% of the carbon dioxide (CO_2) emissions in China (Shan et al., 2018). This drastic increase in fossil fuel energy consumption is accompanied with deterioration of air quality (Chan and Yao, 2008; Fang et al., 2009), posing a threat to public health (Tie et al., 2009; Kan et al., 2012; Chen et al., 2013; Lelieveld et al., 2015). Particulate matter (PM) pollution, especially $PM_{2.5}$ in the North China Plain (NCP), drew public concern and governmental actions (He et al., 2001; Ye et al., 2003; Wang et al., 2005; Sun et al., 2006; Yang et al., 2011; Zhang et al., 2012; Zhang et al., 2013). PM pollution also has complex interactions with the planetary boundary layer (PBL) and its evolution, which can further degrade the air quality (Guo et al., 2016; Li et al., 2017b). Recent studies showed that tropospheric ozone (O_3) pollution increased in China which exacerbated its complex air pollution problem (Xue et al., 2014; Verstraeten et al., 2015; Wang et al., 2017b; Ni et al., 2018).

Elevated ozone concentrations have adverse impacts on both human health (WHO, 2003; Anderson, 2009; Jerrett et al., 2009) and the ecosystem (Adams et al., 1989; Chameides et al., 1999; Ashmore, 2005). Tropospheric ozone absorbs thermal radiation and acts as the third most important anthropogenic contribution to radiative forcing of climate (Ramanathan and Dickinson, 1979; Lacis et al., 1990; IPCC, 2014). In the lower troposphere, the photolysis of ozone is an important source of atmospheric hydroxyl (OH) radicals that control the lifetimes of atmospheric species such as CO and volatile organic compounds (VOCs) (Logan et al., 1981; Thompson, 1992; Finlayson-Pitts and Pitts, 1999). Tropospheric ozone has a relatively long lifetime of several days to weeks (Stevenson et al., 2006; Young et al., 2013), leading to significant long-range transport of ozone and its precursors (Jacob et al., 1999; Derwent et al., 2004; Lin et al., 2008). Thus, investigation of ozone pollution in China is essential to support the national and international policy decision for air quality and the climate.

Tropospheric ozone is produced through complex photochemical reactions of precursors including nitrogen oxides (NO_x = NO + NO_2) and VOCs in the presence of sunlight (Haagensmit, 1952; Crutzen, 1974; Fishman et al., 1979; Seinfeld and Pandis, 2006). In China,

sectors of power generation, industry, and transportation dominates the NO_x emissions (Streets et al., 2003; Ohara et al., 2007; Zhao et al., 2013a). Before 2010, NO_x emissions in China increased substantially (Lin et al., 2010a; Zhao et al., 2013c). Analysis of satellite data revealed that recently NO_x emissions have started decreasing in highly developed regions such as the Pearl River Delta (PRD), but still increased in other regions (Gu et al., 2013; Duncan et al., 2016; Liu et al., 2016). Anthropogenic VOCs emissions had a similar increasing trend in the past decades (Bo et al., 2008; Wei et al., 2011; Kurokawa et al., 2013; Zhao et al., 2017) and are projected to increase in the future (Zhang et al., 2018). Therefore the recent increase of tropospheric ozone in China could likely be explained by the enhanced anthropogenic emissions of ozone precursors.

Due to the complex O_3-NO_x-VOCs chemistry, we need to investigate the photochemical regime for local ozone production, i.e., NO_x-sensitive or VOC-sensitive (Dodge, 1987; Kleinman, 1994). Duncan et al. (2010) used the ratio of tropospheric columns of formaldehyde (HCHO) and nitrogen dioxide (NO_2) observed by the National Aeronautics and Space Administration (NASA) Aura Ozone Monitoring Instrument (OMI) to characterize ozone sensitivity. Studies show that a NO_x-sensitive regime dominates in the United States, except in megacities such as Los Angles and New York City where the local ozone production is in VOC-sensitive or in transition regimes (Duncan et al., 2010; Jin et al., 2017; Ring et al., 2018). However, VOC-sensitive and transition regimes for ozone photochemical production exist ubiquitously in China due to large amount of NO_x emissions, especially over the NCP (Chou et al., 2009; Xing et al., 2011; Jin and Holloway, 2015; Jin et al., 2017). As such, although the current regulations in China focus only on reduction of NO_x emissions (Wang and Hao, 2012; Wang et al., 2014a), air quality might also benefit from VOCs controls.

Aircraft measurements are essential to study the precursor emissions, photochemical production, and transport of ozone pollution at regional scale. However, airborne campaigns are sparse in China (Dickerson et al., 2007; Zhang et al., 2014; Ding et al., 2015; Huang et al., 2015; Wang et al., 2017a). To better understand the characteristics of ozone pollution, the Air Chemistry Research in Asia (ARIAs) aircraft campaign was conducted in Hebei Province of the NCP during May-June 2016, which was affiliated with the surface Aerosol Atmosphere Boundary-Layer Cloud (A^2BC) experiment (Wang et al., 2018a; Wang et al., 2018b). Concentrations of major air pollutants in the lower atmosphere were measured during 11 research flights in the NCP, which were conducted in association with the NASA Korea U.S. –

Air Quality (KORUS-AQ) campaign in downwind South Korea. Measurements collected in the ARIAs research flights and the A^2BC surface observations provide a comprehensive dataset to thoroughly study the tropospheric ozone pollution and emissions of its precursors in China.

In this study, we evaluate anthropogenic emissions and the ozone pollution in the NCP using a combination of aircraft measurements, satellite observations, and modeling results. The U.S. Environmental Protection Agency (EPA) Community Multiscale Air Quality (CMAQ) model was used to simulate the atmospheric chemistry for the ARIAs campaign. We evaluate the emission data by comparing with the aircraft measurements and satellite products, and adjust emissions to improve the CMAQ performance. Lastly, we investigate the sensitivity of ozone production derived from CMAQ simulations and OMI observations and discuss the future ozone pollution in China.

2. Data and Method

2.1 Aircraft campaign in the NCP

With more than 250 million tons of iron and steel produced in 2016 (data from http://data.stats.gov.cn, accessed in September 2018), Hebei Province in the NCP is the most industrialized area in China. Due to its high emissions and proximity to megacities Beijing and Tianjin, the Beijing-Tianjin-Hebei area had severe air pollution in the past decade (Zhao et al., 2013b; Wang et al., 2014b). In May and June 2016, the ARIAs aircraft campaign was conducted over Hebei Province to investigate the emissions, chemical evolution, and transport of air pollutants. The airborne campaign was coordinated with the A^2BC field campaign in Xingtai (XT, 37.18 °N, 114.36 °E, 182 m above sea level, ASL) and the NASA KORUS-AQ campaign to expand the study to East Asia. A Harbin Y12 research airplane (similar to the de Havilland Twin Otter) was employed to measure concentrations of air pollutants including O_3, carbon monoxide (CO), CO_2, NO_2, and aerosol optical properties. The research airplane was located in Luancheng airport, hereafter referred to as LC (LC, 37.91 °N, 114.59 °E, 58 m ASL), south of Shijiazhuang, the capital city of Hebei province with 10 million population. Eleven research flights were conducted during the ARIAs campaign (Fig. S1 in the supplementary material~~a~~). Vertical profiles of air pollutants from near surface (~100 m above ground level, AGL) to the free troposphere (> 3000 m) were conducted over LC, XT (the supersite of the A^2BC campaign), Julu (JL, 37.22 °N,

115.02 °E, 30 m ASL), and Quzhou (QZ, 36.76 °N, 114.96 °E, 40 m ASL).

The airborne measurements of ozone were conducted using a commercially available analyzer (Model 49C, Thermo Environmental Instruments, TEI, Franklin, Massachusetts) (Taubman et al., 2006). NO_2 was measured using a modified commercially available cavity ring-down spectroscopy (CRDS) detector (Castellanos et al., 2009; Brent et al., 2013). Nitrogen oxide (NO) and reactive nitrogen compounds (NO_y) concentrations were analyzed using a commercial available NO analyzer (Model 42C, Thermo Environmental Instruments) with a hot molybdenum convertor working at 375 ^oC (Luke et al., 1992; Stehr et al., 2000). Ambient gas input was switched with and without the convertor frequently to measure NO and NO_y simultaneous. However, due to high power demand of the instrument and convertor, NO and NO_y were only measured during some research flights. Concentrations of CO and CO_2 were monitored with a 4-channel Picarro CRDS instrument (Model G2401-m, Picarro Inc., Santa Clara, CA), calibrated with CO/CO_2 standards certified at the National Institute of Standards and Technology (Ren et al., 2018). All the instruments were routinely serviced, calibrated and used for airborne measurements in the United States and China (Taubman et al., 2006; Dickerson et al., 2007; Hains et al., 2008; He et al., 2012; He et al., 2014; Ren et al., 2018; Salmon et al., 2018). Detailed information about the instrumentation including the sampling frequency, precisions and accuracies is listed in Tables S1 of the supplementary material. Measurements of ambient air pollutants were logged at 1 Hz frequency but the average times for different instruments are different as shown in Table S1. All measurements were synchronized based on the Picaroo measurements of CO_2, and CO with time, geolocation and altitude from the Global Position System (GPS). ~~Measurements of ambient air pollutants were made at 1 Hz frequency and synchronized with time, geolocation and altitude from the Global Position System (GPS).~~ The delay and lag time of each instrument was considered during the post-processing of observation data and averaged to 1-min record for further analysis and model evaluation.

In the ARIAs research flights, 28 whole air samples (WAS) were collected in vertical spirals at different altitudes from ~400 m to ~3500 m. The WAS were analyzed using gas chromatography (GC) with Flame Ionization Detection (FID) and Mass Spectroscopy (MS) by the College of Environmental Sciences and Engineering at Peking University. 74 species of alkanes, alkenes/alkynes, aromatics, and halocarbons were identified and quantified for a study on ozone photochemical chemistry (see details in Benish et al., 2019). Detection limits for the

compounds ranged from 2 to 50 pptv. Surface observation of trace gas pollutions including O_3, CO, NO, and NO_x were measured at the A^2BC Xingtai supersite using analyzers manufactured by Ecotech (Wang et al., 2018b); detailed description of the analyzers is discussed in Zhu et al. (2016). Surface HCHO concentrations were monitored using a formaldehyde analyzer (AERO LASER, Germany, Model 4021) based on fluorometric Hantzsch reactions (Gilpin et al., 1997; Rappenglück et al., 2010). All surface observations were collected as 1-min averaged data and processed to hourly mean values.

2.2 Satellite products

To evaluate the emissions and atmospheric chemistry in the NCP and greater East Asia, we used satellite observations of CO, NO_2, and HCHO for May and June 2016. The Measurements of Pollution In the Troposphere (MOPITT) instrument onboard the NASA Terra satellite retrieved CO column contents with ~10:30 am local overpass time (Deeter et al., 2003). We used the latest version 7 MOPITT Level 3 daily gridded average products (1° × 1° spatial resolution, available at https://eosweb.larc.nasa.gov/project/mopitt/mop03j_v007) for the ARIAs campaign period (MOPITT Science Team, 2013). MOPITT thermal-infrared and near-infrared (TIR + NIR) products shows improved sensitivity to near surface CO in China (Worden et al., 2010). We used MOPITT near surface CO (~ 900 hPa) products and related averaging kernels (AKs) to evaluate the CMAQ results (Deeter et al., 2012).

OMI, onboard the NASA Aura satellite, is a UV/Vis solar backscatter spectrometer in a polar sun-synchronous orbit with a ~1:35 pm local overpass time. With high spatial resolution (13 km × 24 km for the center at nadir) and nearly daily coverage, OMI provided monitoring of trace gases and aerosol properties from 2005 (Levelt et al., 2006). The Version 3 OMI Level 2 NO_2 products (https://disc.gsfc.nasa.gov/datasets/OMNO2_V003/summary) (Krotkov et al., 2018) were used to evaluate the emissions and atmospheric chemistry in East Asia. Under clear sky, tropospheric NO_2 columns from OMI has precision of ~0.5 × 10^{16} molecules cm^{-2} and an accuracy of ±30% (Krotkov et al., 2017). OMI HCHO Version 3 Smithsonian Astronomical Observatory (SAO) (https://disc.gsfc.nasa.gov/datasets/OMHCHO_V003/summary) Level 2 products were used in this study (Chance, 2007; González Abad et al., 2015). The precision of column HCHO is ~1.0 × 10^{16} molecules cm^{-2} and SAO products have an accuracy of ±25-30% without cloud (Millet et al., 2006; Boeke et al., 2011). Data in OMI pixels affected by the row

anomaly and contaminated by clouds were filtered out using quality flags for both NO_2 and HCHO columns.

2.3 Model set-up

We used CMAQ version 5.2 (EPA, 2017) to simulate atmospheric chemistry for the ARIAs campaign. The Weather Research and Forecasting (WRF) model Version 3.8.1 (Skamarock et al., 2008) was driven by the European Centre for Medium-Range Weather Forecasts (ECMWF) ERA-Interim products (ds627.0, https://rda.ucar.edu/datasets/ds627.0) (Dee et al., 2011) to simulate meteorological fields. Two domains with spatial resolution of 36 km and 12 km (Fig. 1~~b~~) were used to cover East Asia, with 35 layers from the surface to 50 hPa and ~20 layers in the lowest 2 km. Major physical options in WRF include the Rapid Radiative Transfer Model (RRTM) radiation scheme (Clough et al., 2005), the Pleim-Xiu surface layer and land surface model (Pleim and Xiu, 1995; Xiu and Pleim, 2001), the Asymmetric Convective Model (ACM2) boundary layer scheme (Pleim, 2007), the Kain-Fritsch cumulus scheme (Kain, 2004), and the WRF Single-Moment 6 (WSM-6) microphysics (Hong and Lim, 2006). The National Centers for Environmental Prediction (NCEP) ADP Global Surface and Upper Air Observational Weather Data (ds461.0 and ds351.0, https://rda.ucar.edu) were used to perform observational and analysis nudging on all domains following the method developed for NASA aircraft campaigns (He et al., 2014; Mazzuca et al., 2016). WRF outputs were processed by the EPA Meteorology-Chemistry Interface Processor Version 4.3 (MCIP v4.3, released in November 2015) for emission processing and CMAQ simulations.

Anthropogenic emissions were from the Emissions Database for Global Atmospheric Research Version 4.2 (EDGAR v4.2, 0.1° × 0.1° resolution) of year 2010, which are widely used for chemical transport modeling (European Commission, 2011). We used the EPA Sparse Matrix Operator Kernel Emissions (SMOKE) modeling system Version 4.5 (UNC, 2017) to project EDGAR emissions to the modeling domain. Emissions of air pollutants were speciated into Carbon Bond 05 chemical mechanism (Yarwood et al., 2005) and updated AERO6 aerosol module (Appel et al., 2013). The EDGAR v4.2 inventory has emissions for energy, industry, residential, and transport sectors. Without stack height information for power plants in the energy sector, we followed the approach developed in He et al. (2012) to locate these anthropogenic emissions at ~200 m above the surface as an approximation for averaged stack height and plume

rise. We used the United States Geological Survey (USGS) 24 category land use dataset combined with the Biogenic Emission Inventory System (BEIS) emission factors table to generate the input files for the CMAQ inline biogenic emissions modeling. Biogenic emissions were estimated using the BEIS module inline in CMAQ (EPA, 2017).

CMAQ v5.2 uses the updated Carbon Bond 6 (CB6r3) chemical mechanism (Yarwood et al., 2010) including improved chemistry mechanism for organic nitrates and peroxyacyl nitrates (PAN) chemistry and will lead to better performance for simulating Secondary Organic Aerosols (SOA) and tropospheric ozone in the United States (Appel et al., 2016). CMAQ was run with a coarse domain and a nested domain (Fig. 1~~b~~). Chemical initial and boundary conditions for the coarse domain were obtained from the default concentration profiles built in CMAQ (EPA, 2017). Results from the CMAQ coarse domain were used to generate boundary conditions for the nested domain. The WRF-CMAQ system was run from mid-April to June with the first 2 weeks as spin-up. Hourly concentrations of air pollutants were saved for further analysis and model evaluation.

3. Results and discussion

3.1 Air Pollution in the NCP and CMAQ performance

Figure 2 summarizes all aircraft measurements of O_3, NO_2, CO, and CO_2 over the NCP from eleven research flights. Generally, we observed high concentrations of air pollutants, with maximum values~~such~~ as >100 part per billion by volume (ppbv) of O_3, >20 ppbv of NO_2, >500 ppbv of CO, and >450 part per million by volume (ppmv) of CO_2, in the aircraft campaign area (defined as 36.5-38.5°N, 114.0-115.5°E hereafter). We conducted vertical spirals over XT (the A^2BC supersite), LC (the airport in south of Shijiazhuang), and two rural areas (JL and QZ) during the ARIAs research flights. Figure 3a summarizes vertical distributions and the mean profiles of air pollutants over XT, with mean O_3 concentrations of 80 ppbv in the lower atmosphere. We observed isolated plumes with >10 ppbv of NO_2, >1000 ppbv of CO, and >440 ppmv of CO_2 over XT, usually with a secondary maximum between 800 and 1200 m (a sample plume was presented in Fig. S2 of the supplementary material). These plumes aloft can play an important role in long-range transport of air pollutants to downwind regions. Profiles over LC (Fig. 3b) show higher O_3 concentrations (>100 ppbv) and relatively moderate NO_2 (~3 ppbv) and

CO (~250 ppbv). The rural areas, JL and QZ, have relatively clean environment with <80 ppbv of O_3, <2 ppbv of NO_2, and <300 ppbv of CO (Fig. 3c and 3d). Even the concentrations of air pollutants over the rural region in the NCP are comparable or higher than values in urban areas in North America and Europe. In summary, we found ~~the~~ both south-north gradient and east-west gradient~~s~~ of air pollution in the campaign region, i.e., higher concentrations of air pollutants in the west XT-LC corridor near the mountain as compared with east side of JL and QZ, and higher concentrations in the north LC as compared with the south XT. Thus, the ARIAs research flights have good coverage of regions with both high and moderate concentrations of air pollutants and can fairly represent the regional nature of air pollution over the NCP.

Comparison of the surface trace gas observations at the Xingtai supersite and the CMAQ simulations driven by the EDGAR inventory (named baseline CMAQ case hereafter) reveals that CMAQ generally underestimates concentrations of major air pollutants (Fig. ~~S1~~ S3 in the supplementary material). The baseline CMAQ run successfully captures the diurnal and daily variations of surface ozone in Xingtai, although consistently underpredicts its concentrations. For CO and NO_x, two important ozone precursors, CMAQ substantially underestimates their concentrations in Xingtai by more than 50% and especially fails to capture the extremely high values such as 6~7 ppmv of CO and ~100 ppbv of NO_x. This underestimation could be caused by local sources poorly represented in the 12-km model simulations. For ambient HCHO, an important byproduct of VOC oxidization in ozone photochemical production, the baseline CMAQ run captures the variations, but substantially underestimates its concentrations. These results suggest that the underestimation of ozone precursors in CMAQ could lead to the poor model performance of simulating tropospheric ozone and other pollutants. It is worth noting that PBL dynamics could also play an important role in accurately simulating the concentrations of air pollutants, especially with the complex terrain at the Xingtai supersite (Figure S4 in the supplementary material). However, evaluation of the PBL simulations and advections in CMAQ is beyond the scope of this study, and we focus on the photochemistry of ozone here.

Similar analyses were conducted to investigate air pollutant concentrations in the lower troposphere over the NCP observed by the aircraft. A case of the research flight on June 11, 2016 (Fig. ~~S2~~ S5 in the supplementary material) shows that CMAQ well captures the vertical gradient of air pollutants, while substantially underestimates concentrations of all trace gases except NO_y. Since CMAQ generated hourly outputs, to alleviate the uncertainty of comparing 1-min aircraft

data and hourly model simulations, we used 10-min averaged aircraft measurements which were matched to the closest hourly model output f~~F~~ollowing the approach described in Goldberg et al. (2016)~~., we calculated the 10-min average O_3, CO, NO, and NO_2 concentrations from aircraft measurements and compared them with the baseline CMAQ simulations (Fig. 4) and~~ Figure 4 ~~found~~ shows~~ similar underestimation (50% to 75% for all air pollutants) as compared with surface measurements (Fig. ~~S1~~ S3 in the supplementary material). CMAQ overestimates NO_y but substantially underestimates NO and NO_2, which suggests that a significant amount of reactive nitrogen compounds could exist in the format of organic nitrates or nitrate aerosols in the model. Figure 5 compares total VOCs concentrations from WAS samples and CMAQ simulations, indicating that VOCs levels are also significantly underestimated by 80%. The model evaluation with surface and aircraft measurements suggest that ~~in the NCP~~ ozone pollution in the NCP has been significantly underestimated in the baseline CMAQ run, which could be due to the uncertainty introduced by using the 2010 EDGAR emissions to simulate the 2016 ARIAs campaign period. Thus, we need to evaluate the emissions inventory data to improve the CMAQ performance and investigate the sensitivity of ozone production.

3.2 Evaluation of emissions inventory in the NCP

The EDGAR v4.2 emission inventory in East Asia was created based on the 2010 MIX emission inventory (Li et al., 2017a), so substantial changes were anticipated when used for the ARIAs campaign in 2016. Anthropogenic emission inventories are usually based on the "bottom-up" approach, which relies on the statistics of fossil fuel usage and emission factors (EFs) for each sector defined as the ratio of the amount of air pollutants released by a unit of CO_2 emissions, e.g. CO/CO_2 and NO_x/CO_2. The 2010 EDGAR inventory has emissions for 4 sectors: Energy, Industry, Transportation, and Residential. We calculated the CO/CO_2, NO_x/CO_2, and NO_x/CO ratios through averaging the EFs from these 4 sectors (Fig. 6).

To evaluate the emission inventory data in the NCP, we used a plume recognition method to calculate the emission enhancements (EEs) from Y12 observations. We first selected 60 1-s aircraft measurements with a 60-s moving window. ~~-~~Then we~~and~~ conducted linear regression of observed air pollutant (CO, NO_x, etc.) concentrations vs. CO_2 concentrations in each 60-s window and calculated the slope~~,~~ (i.e. $\Delta CO/\Delta CO_2$ and $\Delta NO_x/\Delta CO_2$~~,~~) and correlation (R). The slope is defined as ~~emission enhancements (~~EEs~~)~~ in each window, standing for a 'plume' tested

in the 60-s window. Lastly, we ~~Through~~ only ~~selecting~~ selected EEs that are within the PBL (below 1.5 km AGL in this study) and statistically significant ($R^2 > 0.6$), so the values of these selected EEs can act as a proxy of EFs in the air mass observed. The detailed information about this plume recognition method can be found in Halliday et al. (2019) ~~(Halliday et al., 2019)~~.

EEs observed during the research flights have a broad range of values. $\Delta CO/\Delta CO_2$ ranges from below 1%, a typical value of modern automobile emissions, to higher than 10%, a value indicating fossil fuel combustion with high emissions such as biomass burning (Fig. 6a and 6b). The mean of observed EE for CO (3.7%) is close to that calculated from the EDGAR inventory (4.0%) in the aircraft campaign area. Observed $\Delta NO_x/\Delta CO_2$ ratios also have isolated high values (>0.1%) with a mean value of 0.05%, which is substantially higher than the EF (~0.03%) derived from the EDGAR inventory. Since estimation of anthropogenic CO_2 flux in an urban/suburban area is challenging (Cambaliza et al., 2014; Heimburger et al., 2017), the underestimation of CO and NO_x in the NCP could be caused by either underestimated EFs or uncertainty in anthropogenic CO_2 emission data used in the 'bottom-up' approach.

To further investigate the characteristics of air pollutant emissions in the NCP, we conducted a similar analysis of $\Delta NO_x/\Delta CO$, which are usually co-emitted in combustion processes. Since around half of the CO and NO_x are from mobile sources in the EDGAR emission inventory, this ratio can approximately represent the emission characteristic of mobile sources in the NCP. The mean observed $\Delta NO_x/\Delta CO$ ratio is ~1.3%, significantly lower than 5.6% based on the EDGAR emission inventory (Fig. 6c). These results suggest that the EDGAR emission inventory substantially overestimates the ratios of NO_x/CO, while the automobile emissions over the NCP in 2016 have been greatly improved due to recent regulations, i.e., EDGAR overestimates the contribution from combustion with high emissions. It is worth noting that we only evaluated the emission ratios (EEs or EFs) in the EDGAR inventory, while the underestimation of CO and NO_x emissions could be caused by inaccurate CO_2 emissions which have not been examined in this study.

3.3 Evaluation of CO, NO_x, and VOCs emissions using satellite data

Satellite observations are widely used to evaluate the anthropogenic emissions in East Asia sometimes supplemented by model simulations, e.g., CO emissions using the MOPITT CO products (Jiang et al., 2015; Zheng et al., 2018), anthropogenic NO_x emissions using OMI NO_2

products (Wang et al., 2012; de Foy et al., 2015; Qu et al., 2017), and VOCs emissions using OMI HCHO products (Stavrakou et al., 2016). In this study, we used measurements from multiple satellite instruments to evaluate the CMAQ performance of NO_2, HCHO, and CO. Since NO_2 and HCHO can be treated as proxy of NO_x and VOCs emissions, we can further improve the 2010 EDGAR emissions over the NCP base on satellite data.

We followed the approach developed in Canty et al. (2015) to compare the tropospheric column contents of NO_2 from OMI products and CMAQ simulations. Level 2 OMI NO_2 swatch information including row anomaly and quality flags were used to sample NO_2 vertical profiles from CMAQ outputs, and then CMAQ NO_2 column was calculated using the OMI averaging kernel (AK). Lastly, we averaged OMI and CMAQ NO_2 column contents to create daily 0.25° × 0.25° Level 3 products (see details in Canty et al., 2015). A similar approach was used to integrate HCHO column contents from CMAQ simulations based on OMI HCHO retrievals (see details in Ring et al., 2018) and construct daily 0.25° × 0.25° Level 3 HCHO products. For tropospheric CO, we selected the CO concentrations at ~ 900 hPa in CMAQ and averaged them to 1.0° × 1.0° daily products using MOPITT CO averaging kernel (MOPITT Science Team, 2013). All gridded daily data of satellite and CMAQ were averaged in May and June 2016 for comparison.

Figure 7a shows strong signals over the NCP of the OMI NO_2 observations. We plotted OMI and CMAQ NO_2 columns over eastern China and the campaign area (Fig. 8). Generally, NO_2 columns from OMI and CMAQ agreed well over the eastern China (Fig. 8a) but large discrepancies with both overestimation and underestimation existed. For the aircraft campaign area, CMAQ underestimates NO_2 columns (slope = 0.95 and mean ratio = 0.81, i.e., only predicts 81% of OMI NO_2 column) with uncertainties relatively smaller within the 2-month period (Fig. 8b). ~~CMAQ underestimates NO_2 columns over the aircraft campaign area, and only predicts 81% of NO_2 column as compared with OMI observations.~~ However, in urban regions such as Beijing, the Yangtze River Delta (YRD), and the PRD, CMAQ substantially overestimates column NO_2 by up to 30%. Because the baseline CMAQ simulations used the 2010 anthropogenic emission data, these differences should reflect the changes in NO_x emissions due to recent air pollution regulations. The comparison of NO_2 column suggests that NO_x pollution of megacities in China has been substantially improved after 2010 while NO_x pollution in smaller cities and rural area has worsened, consistent with results from independent studies

using OMI (Duncan et al., 2016; Krotkov et al., 2016). OMI HCHO retrievals also show high values over the NCP in spring when plants' photosynthetic activity is relatively low, reflecting that the domination of anthropogenic VOCs emissions in north China (Zhao et al., 2017). CMAQ has good agreement with OMI HCHO within the aircraft campaign area (<20% underestimation), but substantially underestimates HCHO columns in south China where biogenic VOCs dominate (Fig. 7b). The MOPPIT products show high near-surface CO concentrations over the eastern China (Fig. 7c), while the baseline CMAQ run substantially underestimates CO concentrations over north China and only predicts 42% of the CO over the aircraft campaign area.

Using NO_2 and HCHO as proxies of NO_x and VOCs emissions, the comparison of satellite observations and the baseline CMAQ simulations suggests that both NO_x and VOCs emissions in the aircraft campaign area need to be adjusted for a better simulation of tropospheric ozone. Also the underestimation of CO, as an important precursor, can lead to underprediction of tropospheric ozone. We calculated the model/satellite ratios of NO_x, HCHO, and CO in East Asia (Fig. ~~8~~S6 in the supplementary material) and used these ratios to adjust their anthropogenic emissions in CMAQ. The results will be discussed in Section 3.4.

3.~~3~~ 4 Tropospheric ozone production sensitivity from OMI and CMAQ

Photochemical production of tropospheric ozone is highly non-linear and dependent on concentrations of NO_x and VOCs (Kleinman, 1994; Sillman, 1999; Kleinman, 2000). A maximum rate of ozone production can be achieved with an optimal VOCs/NO_x ratio. With other VOCs/NO_x ratios, ozone production can be either in the VOC-sensitive regime (the rate of ozone production is controlled by VOCs concentrations) or in the NO_x-sensitive regime (the rate of production is controlled by NO_x concentrations). Different pollution control strategies can be implemented to reduce the tropospheric ozone levels in these two regimes. For instance, in a VOC-sensitive environment, reducing NO_x emissions will lead to limited effects until the ozone production has been changed to a NO_x-sensitive environment with the continuous remove of NO_x from the atmosphere. Duncan et al. (2010) developed an approach using OMI HCHO/NO_2 column ratio to estimate the ozone production sensitivity as: 1) HCHO/NO_2 < 1: VOC-sensitive regime; 2) HCHO/NO_2 1~2: transition regime; 3) HCNO/NO_2 > 2: NO_x-sensitive regime. Studies show that urban areas in the U.S. such as Los Angeles, New York City and Houston are

in VOC-sensitive or transition regimes, which lead to difficulty in local regulation of air quality (Duncan et al., 2010; Mazzuca et al., 2016; Ring et al., 2018). Recent studies suggest new threshold values of $HCHO/NO_2$ ratios between VOC-sensitive, transition, and NO_x-sensitive regimes in the U.S. (Jin et al., 2017; Schroeder et al., 2017).

Using the Duncan et al. (2010) approach, studies using OMI products suggest large areas of eastern China are either in VOC-sensitive regime (mostly megacities such as Beijing) or in transition regime (Jin and Holloway, 2015; Jin et al., 2017; Xing et al., 2018). We follow the approach described in Ring et al. (2018) to calculate the column $HCHO/NO_2$ ratios from OMI observations and CMAQ simulations for East Asia. OMI column $HCHO/NO_2$ ratios suggest that the ozone photochemical production is VOC-sensitive or in transition region over the NCP and other major urban areas such as YRD and PRD (Fig. 9a) if the Duncan et al. (2010) approach is applicable for these areas. CMAQ successfully captured the spatial distribution of the regional nature of ozone production sensitivity in eastern China, but predicted that the rate of ozone production is controlled more by VOCs with the CMAQ $HCHO/NO_2$ ratio lower than 1.0 in Beijing, YRD, and PRD (Fig. 9b). The VOC-sensitive environment from both OMI observations and CMAQ simulations suggests the rate of ozone photochemical production in the NCP is controlled not only by NO_x emissions, but also by VOCs emissions which currently lack regulations in China. With continuous reduction of anthropogenic NO_x emissions in China, VOCs controls might be efficient in these VOC-sensitive regions.

3.~~4~~ 5 Improvements of tropospheric ozone simulation using satellite products

Results of the previous two sections show that the baseline CMAQ run substantially underestimates the concentrations of ozone and its major precursors in the NCP. Independent studies using KORUS-AQ observations and satellite products suggested that major ozone precursor emissions such as CO and NO_x could have large discrepancies as compared with emission inventory in East Asia (Goldberg et al., 2019; Miyazaki et al., 2019). To identify the individual and combined effects of emission discrepancy of major ozone precursors in the NCP, we designed a series of sensitivity experiments with emissions adjusted to satellite observations. Unlike the top-down approach using global chemical transport models such GEOS-Chem (Lin et al., 2010b; Qu et al., 2017), here we simply applied the ratios of air pollutant column contents from satellite observations and CMAQ simulations on each 0.25 degree grids (Fig. ~~8~~S6 in the

supplementary material) as: CO_{CMAQ}/CO_{MOPITT}, NO_{2CMAQ}/NO_{2OMI}, and $HCHO_{CMAQ}/HCHO_{OMI}$ ratios for anthropogenic CO, NO_x, and VOCs emissions, respectively. To estimate the contribution from biogenic VOCs emissions, we conducted one more run with the in-line BEIS module turned off. Table 1 shows the emission adjustments for the five sensitivity experiments. CMAQ was run for the nested 12 km domain (D02) with the same meteorology, initial conditions, and boundary conditions derived from the coarse domain simulations. We conducted a similar analysis of Figure 4 to investigate the discrepancy between satellite products and CMAQ simulations over the eastern China (Figure S7 in the supplementary material). CMAQ_all run successfully reproduced the column NO_2 and near surface CO in eastern China and column HCHO in the NCP. In southern China where biogenic VOCs dominate, adjusting anthropogenic VOCs emissions showed limited improvements on column HCHO simulations.

Figure 10 presents the evaluation of surface observations with respect to two sensitivity experiments (CMAQ_baseline and CMAQ_all with difference with respect to observations are showed in Figure S8 of the supplementary material;~~,~~ comparison with all CMAQ runs are presented in Fig. ~~S3~~ S9 in the supplementary material). CMAQ still might not capture the extreme high values of surface O_3 and CO (Fig. 10a and 10b) and only improved the model simulations slightly. For instance, the maximum CO concentration from CMAQ simulations are ~1700 ppbv while surface observations have CO peaks higher than 6000 ppbv (Fig. 10b). The adjustments of the emission inventory have improved the model simulations of NO_2/NO (Fig. 10c and 10d) and HCHO (Fig. 10e). During the ARIAs flights, we observed various sources of emissions in the aircraft campaign area such as small factories and biomass burning, which are not included in the EDGAR emission inventory. So the reason for the model underestimation could be that the spatial resolution (12 km) of the nested CMAQ domain cannot represent the detailed emissions and resolve the local air pollution hotspots. However it is worth noting that even our CMAQ system is still not capable to reproduce the surface air quality at Xingtai, the adjustments of EDGAR emissions based on satellite observations reduce the underestimation.

The ARIAs flights covered a large area (~10^4 km^2) in Hebei Province, which represent the regional nature of air pollution over the NCP. A case comparison of CMAQ_All case and Y12 measurements on June 11, 2016 (Fig. 11) shows better results in both concentrations and vertical gradient of air pollutants (compared with Fig. ~~S2~~ S5 in the supplementary material), indicating the effectiveness of improving the emission inventories based on satellite

observations. Table 2 summarizes the model performance of CMAQ as compared with aircraft measurements and scatter plots for each CMAQ sensitivity experiment are showed in Figure S10 of the supplementary material. The adjustments of the EDGAR emissions with satellite observations substantially improved simulations of ozone pollution, with the root mean square error (RSME) decreasing from 25.1 ppbv (the baseline case) to 21.2 ppbv (CMAQ_All case) and the mean ratio of CMAQ simulations to aircraft observations increasing from 0.75 to 0.82. The model performance of CO has also been improved, with the RMSE decreasing from 247.0 ppbv to 203.6 ppbv and the mean ratio increasing from 0.40 to 0.66. For nitrogen compounds including NO_2, NO, and NO_y, the adjustments of EDGAR emissions have small impacts on improving the CMAQ performance. The reason could be that the ozone photochemistry is mainly VOC-sensitive over the NCP, so the adjustments of NO_x emissions have limited impacts close to sources.

4. Conclusions and Discussion

The ARIAs campaign conducted aircraft measurements over the NCP and observed high concentrations of air pollutants including O_3, CO, and ~~NO_x~~nitrogen compounds. CMAQ simulations driven by the 2010 EDGAR emissions substantially underestimate the levels of ozone and its precursors in the campaign region. Analysis of emission enhancements of CO and NO_x with respect to concurrent CO_2 measurements suggests that the usage of the 2010 EDGAR emissions for the 2016 ARIAs campaign could introduce substantial uncertainty due to the recent changes of anthropogenic emissions in China. Comparison of atmospheric columns of NO_2 from CMAQ simulations and satellite observations suggests that NO_x emissions decreased in megacities such as Beijing and Shanghai but increased in rural areas from 2010 to 2016. Similar analysis of HCHO and CO shows that the EDGAR VOCs and CO emissions could be also underestimated in the NCP. $HCHO/NO_2$ column ratio from OMI observations indicates tropospheric ozone production is mainly in the VOC-sensitive regime in the NCP, which is also confirmed by CMAQ simulations. To improve the model performance, we adjusted the EDGAR emissions over East Asia based on satellite observations. Better performance of simulating ozone and its precursors ~~is~~ was achieved, while underestimation still exists.

Both satellite observations and CMAQ simulations indicate that the VOC-sensitive

chemistry dominates the ozone photochemical production in eastern China, so the rate of local ozone production is mainly controlled by the VOCs emissions. In the past few years, despite implementation of control measures mainly on SO_2 and NO_x, ozone concentrations have increased in China. Our study indicated that high NO_x concentrations were pervasive in the PBL over rural areas of the NCP, where anthropogenic VOCs were also abundant. Reducing NO_x emissions is essential to control ozone on the regional scale, but our model simulations indicated that reducing VOCs emissions can lower the rate of photochemical smog production.

Currently, studies and regulations on anthropogenic VOCs emissions in China are lacking, so with expectation of further decreasing NO_x emissions in China, more severe ozone pollution could be anticipated. It is worth noting that even VOCs controls can have beneficial impact on the local rate of ozone production in the VOC-sensitive regime, the ozone levels will not decrease until NO_x emissions are substantially lower, i.e., regulations on VOCs are needed as well as the continuous controls on NO_x emissions in China. These results can also partially explain why ozone pollution emerged in the past few years while $PM_{2.5}$ pollution has been substantially improved with strict regulations on anthropogenic emissions. New datasets such as the updated 'bottom-up' emissions inventory for East Asia and high resolution satellite observations such as TROPOMI products are needed to improve the modeling of ozone pollution in China, which can provide scientific evidence for future national and international regulations on air quality.

Author contribution

X.R., R.D., H.H. and Z.L. designed the aircraft campaign; H.H., X.R., F.W., X.D., and F.L. performed the research flights; Y.W., X.R., and T.Z. conducted the surface observations; H.H., T.P., and Y.H. developed the modeling system; H.H., X.R., and S.B. analyzed the data; H.H., X.R., S.B. and R.D wrote the paper

Acknowledgements

This work was funded by the National Science Foundation of the United States (Grant 1558259). We thank all of the A^2BC and ARIAs research team, especially the flight crew of Hebei Weather Modification Office's Y12 airplane. The flight campaign was conducted in association with the NASA's KORUS-AQ campaign.

References

Adams, R. M., Glyer, J. D., Johnson, S. L., and McCarl, B. A.: A reassessment of the economic-effects of ozone on United-States agriculture, Japca-the Journal of the Air & Waste Management Association, 39, 960-968, 1989.

Anderson, H. R.: Air pollution and mortality: A history, Atmospheric Environment, 43, 142-152, 10.1016/j.atmosenv.2008.09.026, 2009.

Appel, K. W., Pouliot, G. A., Simon, H., Sarwar, G., Pye, H. O. T., Napelenok, S. L., Akhtar, F., and Roselle, S. J.: Evaluation of dust and trace metal estimates from the Community Multiscale Air Quality (CMAQ) model version 5.0, Geoscientific Model Development, 6, 883-899, 10.5194/gmd-6-883-2013, 2013.

Appel, K. W., Napelenok, S. L., Hogrefe, C., Foley, K. M., Pouliot, G., Murphy, B. N., Luecken, D. J., and Heath, N.: Evaluation of the Community Multiscale Air Quality (CMAQ) Model Version 5.2, 2016 CMAS Conference, Chapel Hill, NC., 2016.

Ashmore, M. R.: Assessing the future global impacts of ozone on vegetation, Plant Cell Environ., 28, 949-964, 10.1111/j.1365-3040.2005.01341.x, 2005.

Benish, S. E., He, H., Ren, X., Roberts, S., Salawitch, R. J., Li, Z., Wang, F., Zhang, F., Wang, Y., Shao, M., Lu, S., Pfister, G., Flocke, F., and Dickerson, R.: Observations of Nitrogen Oxides and Volatile Organic Compounds over the North China Plain and Impact on Ozone Formation, Journal of Geophysical Research, undere review, 2019.

Bo, Y., Cai, H., and Xie, S. D.: Spatial and temporal variation of historical anthropogenic NMVOCs emission inventories in China, Atmospheric Chemistry and Physics, 8, 7297-7316, 10.5194/acp-8-7297-2008, 2008.

Boeke, N. L., Marshall, J. D., Alvarez, S., Chance, K. V., Fried, A., Kurosu, T. P., Rappenglück, B., Richter, D., Walega, J., Weibring, P., and Millet, D. B.: Formaldehyde columns from the Ozone Monitoring Instrument: Urban versus background levels and evaluation using aircraft data and a global model, Journal of Geophysical Research: Atmospheres, 116, doi:10.1029/2010JD014870, 2011.

Brent, L. C., Thorn, W. J., Gupta, M., Leen, B., Stehr, J. W., He, H., Arkinson, H. L., Weinheimer, A., Garland, C., Pusede, S. E., Wooldridge, P. J., Cohen, R. C., and Dickerson, R. R.: Evaluation of the use of a commercially available cavity ringdown absorption spectrometer for measuring NO2 in flight, and observations over the Mid-Atlantic States, during DISCOVER-AQ, Journal of Atmospheric Chemistry, 1-19, 10.1007/s10874-013-9265-6, 2013.

Cambaliza, M. O. L., Shepson, P. B., Caulton, D. R., Stirm, B., Samarov, D., Gurney, K. R., Turnbull, J., Davis, K. J., Possolo, A., Karion, A., Sweeney, C., Moser, B., Hendricks, A., Lauvaux, T., Mays, K., Whetstone, J., Huang, J., Razlivanov, I., Miles, N. L., and Richardson, S. J.: Assessment of uncertainties of an aircraft-based mass balance approach for quantifying urban greenhouse gas emissions, Atmospheric Chemistry and Physics, 14, 9029-9050, 10.5194/acp-14-9029-2014, 2014.

Canty, T. P., Hembeck, L., Vinciguerra, T. P., Anderson, D. C., Goldberg, D. L., Carpenter, S. F., Allen, D. J., Loughner, C. P., Salawitch, R. J., and Dickerson, R. R.: Ozone and NOx chemistry in the eastern US: evaluation of CMAQ/CB05 with satellite (OMI) data, Atmospheric Chemistry and Physics, 15, 10965-10982, 10.5194/acp-15-10965-2015, 2015.

Castellanos, P., Luke, W. T., Kelley, P., Stehr, J. W., Ehrman, S. H., and Dickerson, R. R.: Modification of a commercial cavity ring-down spectroscopy NO2 detector for enhanced sensitivity, Review of Scientific Instruments, 80, 113107, 10.1063/1.3244090, 2009.

Chameides, W. L., Li, X. S., Tang, X. Y., Zhou, X. J., Luo, C., Kiang, C. S., St John, J., Saylor, R. D., Liu, S. C., Lam, K. S., Wang, T., and Giorgi, F.: Is ozone pollution affecting crop yields in China?, Geophysical Research Letters, 26, 867-870, 10.1029/1999gl900068, 1999.

Chan, C. K., and Yao, X.: Air pollution in mega cities in China, Atmospheric Environment, 42, 1-42, 10.1016/j.atmosenv.2007.09.003, 2008.

Chance, K.: OMI/Aura Formaldehyde (HCHO) Total Column 1-orbit L2 Swath 13x24 km V003, Greenbelt, MD, USA, Goddard Earth Sciences Data and Information Services Center (GES DISC), Accessed: January 2018, 10.5067/Aura/OMI/DATA2015, 2007.

Chen, Y. Y., Ebenstein, A., Greenstone, M., and Li, H. B.: Evidence on the impact of sustained exposure to air pollution on life expectancy from China's Huai River policy, Proc. Natl. Acad. Sci. U. S. A., 110, 12936-12941, 10.1073/pnas.1300018110, 2013.

Chou, C. C. K., Tsai, C.-Y., Shiu, C.-J., Liu, S. C., and Zhu, T.: Measurement of NOy during Campaign of Air Quality Research in Beijing 2006 (CAREBeijing-2006): Implications for the ozone production efficiency of NOx, Journal of Geophysical Research-Atmospheres, 114, D00g01, 10.1029/2008jd010446, 2009.

Clough, S. A., Shephard, M. W., Mlawer, E. J., Delamere, J. S., Iacono, M. J., Cady-Pereira, K., Boukabara, S., and

Brown, P. D.: Atmospheric radiative transfer modeling: a summary of the AER codes, Journal of Quantitative Spectroscopy and Radiative Transfer, 91, 233-244, https://doi.org/10.1016/j.jqsrt.2004.05.058, 2005.

Crutzen, P. J.: Photochemical reactions initiated by and influencing ozone in unpolluted tropospheric air, Tellus, 26, 47-57, 1974.

de Foy, B., Lu, Z., Streets, D. G., Lamsal, L. N., and Duncan, B. N.: Estimates of power plant NOx emissions and lifetimes from OMI NO2 satellite retrievals, Atmospheric Environment, 116, 1-11, http://dx.doi.org/10.1016/j.atmosenv.2015.05.056, 2015.

Dee, D. P., Uppala, S. M., Simmons, A. J., Berrisford, P., Poli, P., Kobayashi, S., Andrae, U., Balmaseda, M. A., Balsamo, G., Bauer, P., Bechtold, P., Beljaars, A. C. M., van de Berg, L., Bidlot, J., Bormann, N., Delsol, C., Dragani, R., Fuentes, M., Geer, A. J., Haimberger, L., Healy, S. B., Hersbach, H., Hólm, E. V., Isaksen, L., Kållberg, P., Köhler, M., Matricardi, M., McNally, A. P., Monge-Sanz, B. M., Morcrette, J. J., Park, B. K., Peubey, C., de Rosnay, P., Tavolato, C., Thépaut, J. N., and Vitart, F.: The ERA-Interim reanalysis: configuration and performance of the data assimilation system, Q. J. R. Meteorol. Soc., 137, 553-597, 10.1002/qj.828, 2011.

Deeter, M. N., Emmons, L. K., Francis, G. L., Edwards, D. P., Gille, J. C., Warner, J. X., Khattatov, B., Ziskin, D., Lamarque, J. F., Ho, S. P., Yudin, V., Attie, J. L., Packman, D., Chen, J., Mao, D., and Drummond, J. R.: Operational carbon monoxide retrieval algorithm and selected results for the MOPITT instrument, Journal of Geophysical Research-Atmospheres, 108, 4399, 10.1029/2002jd003186, 2003.

Deeter, M. N., Worden, H. M., Edwards, D. P., Gille, J. C., and Andrews, A. E.: Evaluation of MOPITT retrievals of lower-tropospheric carbon monoxide over the United States, Journal of Geophysical Research-Atmospheres, 117, D13306, 10.1029/2012jd017553, 2012.

Derwent, R. G., Stevenson, D. S., Collins, W. J., and Johnson, C. E.: Intercontinental transport and the origins of the ozone observed at surface sites in Europe, Atmospheric Environment, 38, 1891-1901, 10.1016/j.atmosenv.2004.01.008, 2004.

Dickerson, R. R., Li, C., Li, Z., Marufu, L. T., Stehr, J. W., McClure, B., Krotkov, N., Chen, H., Wang, P., Xia, X., Ban, X., Gong, F., Yuan, J., and Yang, J.: Aircraft observations of dust and pollutants over northeast China: Insight into the meteorological mechanisms of transport, Journal of Geophysical Research-Atmospheres, 112, D24s90, 10.1029/2007jd008999, 2007.

Ding, K., Liu, J., Ding, A., Liu, Q., Zhao, T. L., Shi, J., Han, Y., Wang, H., and Jiang, F.: Uplifting of carbon monoxide from biomass burning and anthropogenic sources to the free troposphere in East Asia, Atmospheric Chemistry and Physics, 15, 2843-2866, 10.5194/acp-15-2843-2015, 2015.

Dodge, M.: Chemistry of Oxidant Formation: Implications for Designing Effective Control Strategies U.S. Environmental Protection Agency,Washington, D.C. EPA/600/D-87/114 (NTIS PB87179990), 1987.

Duncan, B. N., Yoshida, Y., Olson, J. R., Sillman, S., Martin, R. V., Lamsal, L., Hu, Y. T., Pickering, K. E., Retscher, C., Allen, D. J., and Crawford, J. H.: Application of OMI observations to a space-based indicator of NOx and VOC controls on surface ozone formation, Atmospheric Environment, 44, 2213-2223, 10.1016/j.atmosenv.2010.03.010, 2010.

Duncan, B. N., Lamsal, L. N., Thompson, A. M., Yoshida, Y., Lu, Z. F., Streets, D. G., Hurwitz, M. M., and Pickering, K. E.: A space-based, high-resolution view of notable changes in urban NOx pollution around the world (2005-2014), Journal of Geophysical Research-Atmospheres, 121, 976-996, 10.1002/2015jd024121, 2016.

EPA: CMAQ (Version 5.2) Scientific Document, Zenodo. http://doi.org/10.5281/zenodo.1167892, 2017.

European Commission: Joint Research Centre (JRC)/Netherlands Environmental Assessment Agency (PBL). Emission Database for Global Atmospheric Research (EDGAR), release version 4.2., available at: http://edgar.jrc.ec.europa.eu (accessed in March 2017), 2011.

Fang, M., Chan, C. K., and Yao, X. H.: Managing air quality in a rapidly developing nation: China, Atmospheric Environment, 43, 79-86, 10.1016/j.atmosenv.2008.09.064, 2009.

Finlayson-Pitts, B. J., and Pitts, J. N.: Chemistry of the Upper and Lower Atmosphere, 1st ed., Academic Press, UK, 1999.

Fishman, J., Solomon, S., and Crutzen, P. J.: Observational and theoretical evidence in support of a significant insitu photo-chemical source of tropospheric ozone, Tellus, 31, 432-446, 1979.

Gilpin, T., Apel, E., Fried, A., Wert, B., Calvert, J., Genfa, Z., Dasgupta, P., Harder, J. W., Heikes, B., Hopkins, B., Westberg, H., Kleindienst, T., Lee, Y.-N., Zhou, X., Lonneman, W., and Sewell, S.: Intercomparison of six ambient [CH2O] measurement techniques, Journal of Geophysical Research: Atmospheres, 102, 21161-21188, 10.1029/97jd01314, 1997.

Goldberg, D. L., Vinciguerra, T. P., Anderson, D. C., Hembeck, L., Canty, T. P., Ehrman, S. H., Martins, D. K., Stauffer, R. M., Thompson, A. M., Salawitch, R. J., and Dickerson, R. R.: CAMx Ozone Source Attribution in the Eastern United States using Guidance from Observations during DISCOVER-AQ Maryland, Geophysical Research Letters, 2015GL067332, 10.1002/2015gl067332, 2016.

Goldberg, D. L., Saide, P. E., Lamsal, L. N., de Foy, B., Lu, Z., Woo, J. H., Kim, Y., Kim, J., Gao, M., Carmichael, G., and Streets, D. G.: A top-down assessment using OMI NO2 suggests an underestimate in the NOx emissions inventory in Seoul, South Korea, during KORUS-AQ, Atmos. Chem. Phys., 19, 1801-1818, 10.5194/acp-19-1801-2019, 2019.

González Abad, G., Liu, X., Chance, K., Wang, H., Kurosu, T. P., and Suleiman, R.: Updated Smithsonian Astrophysical Observatory Ozone Monitoring Instrument (SAO OMI) formaldehyde retrieval, Atmos. Meas. Tech., 8, 19-32, 10.5194/amt-8-19-2015, 2015.

Gu, D. S., Wang, Y. H., Smeltzer, C., and Liu, Z.: Reduction in NOx Emission Trends over China: Regional and Seasonal Variations, Environmental Science & Technology, 47, 12912-12919, 10.1021/es401727e, 2013.

Guan, D. B., Meng, J., Reiner, D. M., Zhang, N., Shan, Y. L., Mi, Z. F., Shao, S., Liu, Z., Zhang, Q., and Davis, S. J.: Structural decline in China's CO2 emissions through transitions in industry and energy systems, Nature Geoscience, 11, 551-+, 10.1038/s41561-018-0161-1, 2018.

Guo, J., Miao, Y., Zhang, Y., Liu, H., Li, Z., Zhang, W., He, J., Lou, M., Yan, Y., Bian, L., and Zhai, P.: The climatology of planetary boundary layer height in China derived from radiosonde and reanalysis data, Atmos. Chem. Phys., 16, 13309-13319, 10.5194/acp-16-13309-2016, 2016.

Haagensmit, A. J.: Chemistry and physiology of Los-Angeles smog, Industrial and Engineering Chemistry, 44, 1342-1346, 10.1021/ie50510a045, 1952.

Hains, J. C., Taubman, B. F., Thompson, A. M., Stehr, J. W., Marufu, L. T., Doddridge, B. G., and Dickerson, R. R.: Origins of chemical pollution derived from Mid-Atlantic aircraft profiles using a clustering technique, Atmospheric Environment, 42, 1727-1741, 10.1016/j.atmosenv.2007.11.052, 2008.

Halliday, H. S., DiGangi, J. P., Choi, Y., Diskin, G. S., Pusede, S. E., Rana, M., Nowak, J. B., Knote, C., Ren, X., He, H., Dickerson, R. R., and Li, Z.: Using Short-Term CO/CO2 Ratios to Assess Air Mass Differences over the Korean Peninsula during KORUS-AQ, Journal of Geophysical Research: Atmospheres, 0, 10.1029/2018jd029697, 2019.

He, H., Li, C., Loughner, C. P., Li, Z., Krotkov, N. A., Yang, K., Wang, L., Zheng, Y., Bao, X., Zhao, G., and Dickerson, R. R.: SO2 over central China: Measurements, numerical simulations and the tropospheric sulfur budget, Journal of Geophysical Research: Atmospheres, 117, doi:10.1029/2011JD016473, 2012.

He, H., Loughner, C. P., Stehr, J. W., Arkinson, H. L., Brent, L. C., Follette-Cook, M. B., Tzortziou, M. A., Pickering, K. E., Thompson, A. M., Martins, D. K., Diskin, G. S., Anderson, B. E., Crawford, J. H., Weinheimer, A. J., Lee, P., Hains, J. C., and Dickerson, R. R.: An elevated reservoir of air pollutants over the Mid-Atlantic States during the 2011 DISCOVER-AQ campaign: Airborne measurements and numerical simulations, Atmospheric Environment, 85, 18-30, 10.1016/j.atmosenv.2013.11.039, 2014.

He, K. B., Yang, F. M., Ma, Y. L., Zhang, Q., Yao, X. H., Chan, C. K., Cadle, S., Chan, T., and Mulawa, P.: The characteristics of PM2.5 in Beijing, China, Atmospheric Environment, 35, 4959-4970, 10.1016/s1352-2310(01)00301-6, 2001.

Heimburger, A. M. F., Harvey, R. M., Shepson, P. B., Stirm, B. H., Gore, C., Turnbull, J., Cambaliza, M. O. L., Salmon, O. E., Kerlo, A. E. M., Lavoie, T. N., Davis, K. J., Lauvaux, T., Karion, A., Sweeney, C., Brewer, W. A., Hardesty, R. M., and Gurney, K. R.: Assessing the optimized precision of the aircraft mass balance method for measurement of urban greenhouse gas emission rates through averaging, Elementa-Science of the Anthropocene, 5, 26, 10.1525/elementa.134, 2017.

Hong, S.-Y., and Lim, J.-O.: The WRF single-moment 6-class microphysics scheme (WSM6), J. Korean Meteor. Soc., 42, 129-151, 2006.

Huang, J., Liu, H., Crawford, J. H., Chan, C., Considine, D. B., Zhang, Y., Zheng, X., Zhao, C., Thouret, V., Oltmans, S. J., Liu, S. C., Jones, D. B. A., Steenrod, S. D., and Damon, M. R.: Origin of springtime ozone enhancements in the lower troposphere over Beijing: in situ measurements and model analysis, Atmospheric Chemistry and Physics, 15, 5161-5179, 10.5194/acp-15-5161-2015, 2015.

IPCC: Climate Change 2014: Synthesis Report. Contribution of Working Groups I, II and III to the Fifth Assessment Report of the Intergovernmental Panel on Climate Change [Core Writing Team, R.K. Pachauri and L.A. Meyer (eds.)], IPCC, Geneva, Switzerland, 151 pp., 2014.

Jacob, D. J., Logan, J. A., and Murti, P. P.: Effect of rising Asian emissions on surface ozone in the United States, Geophysical Research Letters, 26, 2175-2178, 10.1029/1999gl900450, 1999.

Jerrett, M., Burnett, R. T., Pope, C. A., Ito, K., Thurston, G., Krewski, D., Shi, Y. L., Calle, E., and Thun, M.: Long-

Term Ozone Exposure and Mortality, N. Engl. J. Med., 360, 1085-1095, 10.1056/NEJMoa0803894, 2009.
Jiang, Z., Worden, J. R., Jones, D. B. A., Lin, J. T., Verstraeten, W. W., and Henze, D. K.: Constraints on Asian ozone using Aura TES, OMI and Terra MOPITT, Atmospheric Chemistry and Physics, 15, 99-112, 10.5194/acp-15-99-2015, 2015.
Jin, X., and Holloway, T.: Spatial and temporal variability of ozone sensitivity over China observed from the Ozone Monitoring Instrument, Journal of Geophysical Research: Atmospheres, 120, 7229-7246, doi:10.1002/2015JD023250, 2015.
Jin, X., Fiore, A. M., Murray, L. T., Valin, L. C., Lamsal, L. N., Duncan, B., Folkert Boersma, K., De Smedt, I., Abad, G. G., Chance, K., and Tonnesen, G. S.: Evaluating a Space-Based Indicator of Surface Ozone-NOx-VOC Sensitivity Over Midlatitude Source Regions and Application to Decadal Trends, Journal of Geophysical Research: Atmospheres, 122, 10,439-410,461, doi:10.1002/2017JD026720, 2017.
Kain, J. S.: The Kain-Fritsch convective parameterization: An update, Journal of Applied Meteorology, 43, 170-181, 2004.
Kan, H. D., Chen, R. J., and Tong, S. L.: Ambient air pollution, climate change, and population health in China, Environ. Int., 42, 10-19, 10.1016/j.envint.2011.03.003, 2012.
Kleinman, L. I.: Low and high NOx tropospheric photochemistry, Journal of Geophysical Research-Atmospheres, 99, 16831-16838, 10.1029/94jd01028, 1994.
Kleinman, L. I.: Ozone process insights from field experiments - part II: Observation-based analysis for ozone production, Atmospheric Environment, 34, 2023-2033, 10.1016/s1352-2310(99)00457-4, 2000.
Krotkov, N. A., McLinden, C. A., Li, C., Lamsal, L. N., Celarier, E. A., Marchenko, S. V., Swartz, W. H., Bucsela, E. J., Joiner, J., Duncan, B. N., Boersma, K. F., Veefkind, J. P., Levelt, P. F., Fioletov, V. E., Dickerson, R. R., He, H., Lu, Z. F., and Streets, D. G.: Aura OMI observations of regional SO2 and NO2 pollution changes from 2005 to 2015, Atmospheric Chemistry and Physics, 16, 4605-4629, 10.5194/acp-16-4605-2016, 2016.
Krotkov, N. A., Lamsal, L. N., Celarier, E. A., Swartz, W. H., Marchenko, S. V., Bucsela, E. J., Chan, K. L., Wenig, M., and Zara, M.: The version 3 OMI NO2 standard product, Atmos. Meas. Tech., 10, 3133-3149, 10.5194/amt-10-3133-2017, 2017.
Krotkov, N. A., Lamsal, L. N., Marchenko, S. V., Celarier, E. A., bucsela, E. J., Swartz, W. H., and Veefkind, J. P.: OMI/Aura Nitrogen Dioxide (NO2) Total and Tropospheric Column 1-orbit L2 Swath 13x24 km V003, Greenbelt, MD, USA, Goddard Earth Sciences Data and Information Services Center (GES DISC), Accessed: January 2018, 10.5067/Aura/OMI/DATA2017, 2018.
Kurokawa, J., Ohara, T., Morikawa, T., Hanayama, S., Janssens-Maenhout, G., Fukui, T., Kawashima, K., and Akimoto, H.: Emissions of air pollutants and greenhouse gases over Asian regions during 2000-2008: Regional Emission inventory in ASia (REAS) version 2, Atmospheric Chemistry and Physics, 13, 11019-11058, 10.5194/acp-13-11019-2013, 2013.
Lacis, A. A., Wuebbles, D. J., and Logan, J. A.: Radiative forcing of climate by changes in the vertical-distribution of ozone, Journal of Geophysical Research-Atmospheres, 95, 9971-9981, 10.1029/JD095iD07p09971, 1990.
Lelieveld, J., Evans, J. S., Fnais, M., Giannadaki, D., and Pozzer, A.: The contribution of outdoor air pollution sources to premature mortality on a global scale, Nature, 525, 367-+, 10.1038/nature15371, 2015.
Levelt, P. F., Hilsenrath, E., Leppelmeier, G. W., van den Oord, G. H. J., Bhartia, P. K., Tamminen, J., de Haan, J. F., and Veefkind, J. P.: Science objectives of the Ozone Monitoring Instrument, Ieee Transactions on Geoscience and Remote Sensing, 44, 1199-1208, 10.1109/tgrs.2006.872336, 2006.
Li, M., Zhang, Q., Kurokawa, J., Woo, J. H., He, K. B., Lu, Z. F., Ohara, T., Song, Y., Streets, D. G., Carmichael, G. R., Cheng, Y. F., Hong, C. P., Huo, H., Jiang, X. J., Kang, S. C., Liu, F., Su, H., and Zheng, B.: MIX: a mosaic Asian anthropogenic emission inventory under the international collaboration framework of the MICS-Asia and HTAP, Atmospheric Chemistry and Physics, 17, 935-963, 10.5194/acp-17-935-2017, 2017a.
Li, Z., Guo, J., Ding, A., Liao, H., Liu, J., Sun, Y., Wang, T., Xue, H., Zhang, H., and Zhu, B.: Aerosol and boundary-layer interactions and impact on air quality, National Science Review, 4, 810-833, 10.1093/nsr/nwx117, 2017b.
Lin, J., Nielsen, C. P., Zhao, Y., Lei, Y., Liu, Y., and McElroy, M. B.: Recent Changes in Particulate Air Pollution over China Observed from Space and the Ground: Effectiveness of Emission Control, Environmental Science & Technology, 44, 7771-7776, 10.1021/es101094t, 2010a.
Lin, J. T., Wuebbles, D. J., and Liang, X. Z.: Effects of intercontinental transport on surface ozone over the United States: Present and future assessment with a global model, Geophysical Research Letters, 35, L02805, 10.1029/2007gl031415, 2008.

Lin, J. T., McElroy, M. B., and Boersma, K. F.: Constraint of anthropogenic NOx emissions in China from different sectors: a new methodology using multiple satellite retrievals, Atmospheric Chemistry and Physics, 10, 63-78, 10.5194/acp-10-63-2010, 2010b.
Liu, F., Zhang, Q., Ronald, J. V., Zheng, B., Tong, D., Yan, L., Zheng, Y. X., and He, K. B.: Recent reduction in NOx emissions over China: synthesis of satellite observations and emission inventories, Environ. Res. Lett., 11, 114002, 10.1088/1748-9326/11/11/114002, 2016.
Logan, J. A., Prather, M. J., Wofsy, S. C., and McElroy, M. B.: Tropospheric chemistry - a global perspective, Journal of Geophysical Research-Oceans and Atmospheres, 86, 7210-7254, 10.1029/JC086iC08p07210, 1981.
Luke, W. T., Dickerson, R. R., Ryan, W. F., Pickering, K. E., and Nunnermacker, L. J.: Tropospheric chemistry over the lower Great-Plains of the United States. 2 Trace gas profiles and distributions, Journal of Geophysical Research-Atmospheres, 97, 20647-20670, 1992.
Mazzuca, G. M., Ren, X. R., Loughner, C. P., Estes, M., Crawford, J. H., Pickering, K. E., Weinheimer, A. J., and Dickerson, R. R.: Ozone production and its sensitivity to NOx and VOCs: results from the DISCOVER-AQ field experiment, Houston 2013, Atmospheric Chemistry and Physics, 16, 14463-14474, 10.5194/acp-16-14463-2016, 2016.
Millet, D. B., Jacob, D. J., Turquety, S., Hudman, R. C., Wu, S., Fried, A., Walega, J., Heikes, B. G., Blake, D. R., Singh, H. B., Anderson, B. E., and Clarke, A. D.: Formaldehyde distribution over North America: Implications for satellite retrievals of formaldehyde columns and isoprene emission, Journal of Geophysical Research: Atmospheres, 111, doi:10.1029/2005JD006853, 2006.
Miyazaki, K., Sekiya, T., Fu, D., Bowman, K. W., Kulawik, S. S., Sudo, K., Walker, T., Kanaya, Y., Takigawa, M., Ogochi, K., Eskes, H., Boersma, K. F., Thompson, A. M., Gaubert, B., Barre, J., and Emmons, L. K.: Balance of Emission and Dynamical Controls on Ozone During the Korea-United States Air Quality Campaign From Multiconstituent Satellite Data Assimilation, Journal of Geophysical Research: Atmospheres, 124, 387-413, 10.1029/2018jd028912, 2019.
MOPITT Science Team: MOPITT/Terra Level 3 Gridded Daily CO (on a latitude/longitude/pressure grid) derived from Near and Thermal Infrared Radiances, version 7, Hampton, VA, USA:NASA Atmospheric Science Data Center (ASDC), Accessed January 2018, 10.5067/TERRA/MOPITT/MOP03J_L3.007, 2013.
Ni, R. J., Lin, J. T., Yan, Y. Y., and Lin, W. L.: Foreign and domestic contributions to springtime ozone over China, Atmospheric Chemistry and Physics, 18, 11447-11469, 10.5194/acp-18-11447-2018, 2018.
Ohara, T., Akimoto, H., Kurokawa, J., Horii, N., Yamaji, K., Yan, X., and Hayasaka, T.: An Asian emission inventory of anthropogenic emission sources for the period 1980-2020, Atmospheric Chemistry and Physics, 7, 4419-4444, 10.5194/acp-7-4419-2007, 2007.
Pleim, J. E., and Xiu, A.: Development and Testing of a Surface Flux and Planetary Boundary Layer Model for Application in Mesoscale Models, Journal of Applied Meteorology, 34, 16-32, 10.1175/1520-0450-34.1.16, 1995.
Pleim, J. E.: A Combined Local and Nonlocal Closure Model for the Atmospheric Boundary Layer. Part I: Model Description and Testing, J. Appl. Meteorol. Climatol., 46, 1383-1395, 10.1175/jam2539.1, 2007.
Qu, Z., Henze, D. K., Capps, S. L., Wang, Y., Xu, X. G., Wang, J., and Keller, M.: Monthly top-down NOx emissions for China (2005-2012): A hybrid inversion method and trend analysis, Journal of Geophysical Research-Atmospheres, 122, 4600-4625, 10.1002/2016jd025852, 2017.
Ramanathan, V., and Dickinson, R. E.: Role of stratospheric ozone in the zonal and seasonal radiative energy-balance of the Earth-troposphere system, Journal of the Atmospheric Sciences, 36, 1084-1104, 1979.
Rappenglück, B., Dasgupta, P. K., Leuchner, M., Li, Q., and Luke, W.: Formaldehyde and its relation to CO, PAN, and SO₂ in the Houston-Galveston airshed, Atmos. Chem. Phys., 10, 2413-2424, 10.5194/acp-10-2413-2010, 2010.
Ren, X., Salmon, O. E., Hansford, J. R., Ahn, D., Hall, D., Benish, S. E., Stratton, P. R., He, H., Sahu, S., Grimes, C., Heimburger, A. M. F., Martin, C. R., Cohen, M. D., Stunder, B., Salawitch, R. J., Ehrman, S. H., Shepson, P. B., and Dickerson, R. R.: Methane Emissions From the Baltimore-Washington Area Based on Airborne Observations: Comparison to Emissions Inventories, Journal of Geophysical Research: Atmospheres, 0, doi:10.1029/2018JD028851, 2018.
Ring, A. M., Canty, T. P., Anderson, D. C., Vinciguerra, T. P., He, H., Goldberg, D. L., Ehrman, S. H., Dickerson, R. R., and Salawitch, R. J.: Evaluating commercial marine emissions and their role in air quality policy using observations and the CMAQ model, Atmospheric Environment, 173, 96-107, https://doi.org/10.1016/j.atmosenv.2017.10.037, 2018.
Salmon, O. E., Shepson, P. B., Ren, X., He, H., Hall, D. L., Dickerson, R. R., Stirm, B. H., Brown, S. S., Fibiger, D.

L., McDuffie, E. E., Campos, T. L., Gurney, K. R., and Thornton, J. A.: Top-Down Estimates of NOx and CO Emissions From Washington, D.C.-Baltimore During the WINTER Campaign, Journal of Geophysical Research: Atmospheres, 123, 7705-7724, doi:10.1029/2018JD028539, 2018.

Schroeder, J. R., Crawford, J. H., Fried, A., Walega, J., Weinheimer, A., Wisthaler, A., Muller, M., Mikoviny, T., Chen, G., Shook, M., Blake, D. R., and Tonnesen, G. S.: New insights into the column CH2O/NO2 ratio as an indicator of near-surface ozone sensitivity, Journal of Geophysical Research-Atmospheres, 122, 8885-8907, 10.1002/2017jd026781, 2017.

Seinfeld, J. H., and Pandis, S. N.: Atmospheric Chemistry and Physics: From Air Pollution to Climate Change, 2nd ed., John Wiley & Sons, Inc., 2006.

Shan, Y., Guan, D., Zheng, H., Ou, J., Li, Y., Meng, J., Mi, Z., Liu, Z., and Zhang, Q.: China CO2 emission accounts 1997–2015, Scientific Data, 5, 170201, 10.1038/sdata.2017.201, https://www.nature.com/articles/sdata2017201#supplementary-information, 2018.

Sillman, S.: The relation between ozone, NOx and hydrocarbons in urban and polluted rural environments, Atmospheric Environment, 33, 1821-1845, 10.1016/s1352-2310(98)00345-8, 1999.

Skamarock, W. C., Klemp, J. B., Dudhia, J., Gill, D. O., Barker, D. M., Duda, M. G., Huang, X.-Y., Wang, W., and Powers, J. G.: A Description of the Advanced Research WRF Version 3, NCAR Technical Note, NCAR/TN-475+STR, 113 pp, 2008.

Stavrakou, T., Muller, J. F., Bauwens, M., De Smedt, I., Lerot, C., Van Roozendael, M., Coheur, P. F., Clerbaux, C., Boersma, K. F., van der A, R., and Song, Y.: Substantial Underestimation of Post-Harvest Burning Emissions in the North China Plain Revealed by Multi-Species Space Observations, Scientific Reports, 6, 32307, 10.1038/srep32307, 2016.

Stehr, J. W., Dickerson, R. R., Hallock-Waters, K. A., Doddridge, B. G., and Kirk, D.: Observations of NOy, CO, and SO2 and the origin of reactive nitrogen in the eastern United States, Journal of Geophysical Research-Atmospheres, 105, 3553-3563, 2000.

Stevenson, D. S., Dentener, F. J., Schultz, M. G., Ellingsen, K., van Noije, T. P. C., Wild, O., Zeng, G., Amann, M., Atherton, C. S., Bell, N., Bergmann, D. J., Bey, I., Butler, T., Cofala, J., Collins, W. J., Derwent, R. G., Doherty, R. M., Drevet, J., Eskes, H. J., Fiore, A. M., Gauss, M., Hauglustaine, D. A., Horowitz, L. W., Isaksen, I. S. A., Krol, M. C., Lamarque, J. F., Lawrence, M. G., Montanaro, V., Muller, J. F., Pitari, G., Prather, M. J., Pyle, J. A., Rast, S., Rodriguez, J. M., Sanderson, M. G., Savage, N. H., Shindell, D. T., Strahan, S. E., Sudo, K., and Szopa, S.: Multimodel ensemble simulations of present-day and near-future tropospheric ozone, Journal of Geophysical Research-Atmospheres, 111, D08301, 10.1029/2005jd006338, 2006.

Streets, D. G., Bond, T. C., Carmichael, G. R., Fernandes, S. D., Fu, Q., He, D., Klimont, Z., Nelson, S. M., Tsai, N. Y., Wang, M. Q., Woo, J. H., and Yarber, K. F.: An inventory of gaseous and primary aerosol emissions in Asia in the year 2000, Journal of Geophysical Research-Atmospheres, 108, 8809, 10.1029/2002jd003093, 2003.

Sun, Y. L., Zhuang, G. S., Tang, A. H., Wang, Y., and An, Z. S.: Chemical characteristics of PM2.5 and PM10 in haze-fog episodes in Beijing, Environmental Science & Technology, 40, 3148-3155, 10.1021/es051533g, 2006.

Taubman, B. F., Hains, J. C., Thompson, A. M., Marufu, L. T., Doddridge, B. G., Stehr, J. W., Piety, C. A., and Dickerson, R. R.: Aircraft vertical profiles of trace gas and aerosol pollution over the mid-Atlantic United States: Statistics and meteorological cluster analysis, Journal of Geophysical Research-Atmospheres, 111, D10s07 10.1029/2005jd006196, 2006.

Thompson, A. M.: The oxidizing capacity of the Earth's Atmosphere - probable past and future changes, Science, 256, 1157-1165, 10.1126/science.256.5060.1157, 1992.

Tie, X. X., Wu, D., and Brasseur, G.: Lung cancer mortality and exposure to atmospheric aerosol particles in Guangzhou, China, Atmospheric Environment, 43, 2375-2377, 10.1016/j.atmosenv.2009.01.036, 2009.

UNC: SMOKE v4.5 User's Manual, The Institute fot the Environment, The University of North Carolina at Chapel Hill, 2017.

Verstraeten, W. W., Neu, J. L., Williams, J. E., Bowman, K. W., Worden, J. R., and Boersma, K. F.: Rapid increases in tropospheric ozone production and export from China, Nature Geoscience, 8, 690-+, 10.1038/ngeo2493, 2015.

Wang, F., Li, Z., Ren, X., Jiang, Q., He, H., Dickerson, R. R., Dong, X., and Lv, F.: Vertical distributions of aerosol optical properties during the spring 2016 ARIAs airborne campaign in the North China Plain, Atmos. Chem. Phys., 18, 8995-9010, 10.5194/acp-18-8995-2018, 2018a.

Wang, R., Xu, X. B., Jia, S. H., Ma, R. S., Ran, L., Deng, Z. Z., Lin, W. L., Wang, Y., and Ma, Z. Q.: Lower

tropospheric distributions of O-3 and aerosol over Raoyang, a rural site in the North China Plain, Atmospheric Chemistry and Physics, 17, 3891-3903, 10.5194/acp-17-3891-2017, 2017a.
Wang, S. W., Zhang, Q., Streets, D. G., He, K. B., Martin, R. V., Lamsal, L. N., Chen, D., Lei, Y., and Lu, Z.: Growth in NOx emissions from power plants in China: bottom-up estimates and satellite observations, Atmospheric Chemistry and Physics, 12, 4429-4447, 10.5194/acp-12-4429-2012, 2012.
Wang, S. X., and Hao, J. M.: Air quality management in China: Issues, challenges, and options, J. Environ. Sci., 24, 2-13, 10.1016/s1001-0742(11)60724-9, 2012.
Wang, S. X., Xing, J., Zhao, B., Jang, C., and Hao, J. M.: Effectiveness of national air pollution control policies on the air quality in metropolitan areas of China, J. Environ. Sci., 26, 13-22, 10.1016/s1001-0742(13)60381-2, 2014a.
Wang, T., Xue, L. K., Brimblecombe, P., Lam, Y. F., Li, L., and Zhang, L.: Ozone pollution in China: A review of concentrations, meteorological influences, chemical precursors, and effects, Science of the Total Environment, 575, 1582-1596, 10.1016/j.scitotenv.2016.10.081, 2017b.
Wang, Y., Zhuang, G. S., Tang, A. H., Yuan, H., Sun, Y. L., Chen, S. A., and Zheng, A. H.: The ion chemistry and the source of PM2.5 aerosol in Beijing, Atmospheric Environment, 39, 3771-3784, 10.1016/j.atmosenv.2005.03.013, 2005.
Wang, Y., Li, Z., Zhang, Y., Du, W., Zhang, F., Tan, H., Xu, H., Fan, T., Jin, X., Fan, X., Dong, Z., Wang, Q., and Sun, Y.: Characterization of aerosol hygroscopicity, mixing state, and CCN activity at a suburban site in the central North China Plain, Atmos. Chem. Phys., 18, 11739-11752, 10.5194/acp-18-11739-2018, 2018b.
Wang, Y. S., Yao, L., Wang, L. L., Liu, Z. R., Ji, D. S., Tang, G. Q., Zhang, J. K., Sun, Y., Hu, B., and Xin, J. Y.: Mechanism for the formation of the January 2013 heavy haze pollution episode over central and eastern China, Sci. China-Earth Sci., 57, 14-25, 10.1007/s11430-013-4773-4, 2014b.
Wei, W., Wang, S. X., Hao, J. M., and Cheng, S. Y.: Projection of anthropogenic volatile organic compounds (VOCs) emissions in China for the period 2010-2020, Atmospheric Environment, 45, 6863-6871, 10.1016/j.atmosenv.2011.01.013, 2011.
WHO: Health aspects of air pollution with particulate matter, ozone and nitrogen dioxide, Wolrd Health Organisation, Bonn,, 2003.
Worden, H. M., Deeter, M. N., Edwards, D. P., Gille, J. C., Drummond, J. R., and Nedelec, P.: Observations of near-surface carbon monoxide from space using MOPITT multispectral retrievals, Journal of Geophysical Research-Atmospheres, 115, D18314, 10.1029/2010jd014242, 2010.
Xing, J., Wang, S. X., Jang, C., Zhu, Y., and Hao, J. M.: Nonlinear response of ozone to precursor emission changes in China: a modeling study using response surface methodology, Atmospheric Chemistry and Physics, 11, 5027-5044, 10.5194/acp-11-5027-2011, 2011.
Xing, J., Ding, D., Wang, S. X., Zhao, B., Jang, C., Wu, W. J., Zhang, F. F., Zhu, Y., and Hao, J. M.: Quantification of the enhanced effectiveness of NOx control from simultaneous reductions of VOC and NH3 for reducing air pollution in the Beijing-Tianjin-Hebei region, China, Atmospheric Chemistry and Physics, 18, 7799-7814, 10.5194/acp-18-7799-2018, 2018.
Xiu, A., and Pleim, J. E.: Development of a Land Surface Model. Part I: Application in a Mesoscale Meteorological Model, Journal of Applied Meteorology, 40, 192-209, 10.1175/1520-0450(2001)040<0192:doalsm>2.0.co;2, 2001.
Xue, L. K., Wang, T., Gao, J., Ding, A. J., Zhou, X. H., Blake, D. R., Wang, X. F., Saunders, S. M., Fan, S. J., Zuo, H. C., Zhang, Q. Z., and Wang, W. X.: Ground-level ozone in four Chinese cities: precursors, regional transport and heterogeneous processes, Atmospheric Chemistry and Physics, 14, 13175-13188, 10.5194/acp-14-13175-2014, 2014.
Yang, F., Tan, J., Zhao, Q., Du, Z., He, K., Ma, Y., Duan, F., and Chen, G.: Characteristics of PM2.5 speciation in representative megacities and across China, Atmospheric Chemistry and Physics, 11, 5207-5219, 10.5194/acp-11-5207-2011, 2011.
Yarwood, G. S., Rao, S. T., Yocke, M., and Whitten, G. Z.: Updates to the Carbon Bond Chemical Mechanism: CB05, ENVIRON International Corp, 2005.
Yarwood, G. S., Whitten, G. Z., Jung, J., Heo, G., and Allen, D.: Development, Evaluation and Testing of Version 6 of the Carbon Bond Chemical Mechanism (CB6), https://www.tceq.texas.gov/assets/public/implementation/air/am/contracts/reports/pm/5820784005FY1026-20100922-environ-cb6.pdf, 2010.
Ye, B. M., Ji, X. L., Yang, H. Z., Yao, X. H., Chan, C. K., Cadle, S. H., Chan, T., and Mulawa, P. A.: Concentration and chemical composition of PM2.5 in Shanghai for a 1-year period, Atmospheric Environment, 37, 499-510, Pii s1352-2310(02)00918-4, 10.1016/s1352-2310(02)00918-4, 2003.

Young, P. J., Archibald, A. T., Bowman, K. W., Lamarque, J. F., Naik, V., Stevenson, D. S., Tilmes, S., Voulgarakis, A., Wild, O., Bergmann, D., Cameron-Smith, P., Cionni, I., Collins, W. J., Dalsoren, S. B., Doherty, R. M., Eyring, V., Faluvegi, G., Horowitz, L. W., Josse, B., Lee, Y. H., MacKenzie, I. A., Nagashima, T., Plummer, D. A., Righi, M., Rumbold, S. T., Skeie, R. B., Shindell, D. T., Strode, S. A., Sudo, K., Szopa, S., and Zeng, G.: Pre-industrial to end 21st century projections of tropospheric ozone from the Atmospheric Chemistry and Climate Model Intercomparison Project (ACCMIP), Atmospheric Chemistry and Physics, 13, 2063-2090, 10.5194/acp-13-2063-2013, 2013.

Zhang, J. N., Xiao, J. F., Chen, X. F., Liang, X. M., Fan, L. Y., and Ye, D. Q.: Allowance and allocation of industrial volatile organic compounds emission in China for year 2020 and 2030, J. Environ. Sci., 69, 155-165, 10.1016/j.jes.2017.10.003, 2018.

Zhang, R., Jing, J., Tao, J., Hsu, S. C., Wang, G., Cao, J., Lee, C. S. L., Zhu, L., Chen, Z., Zhao, Y., and Shen, Z.: Chemical characterization and source apportionment of PM2.5 in Beijing: seasonal perspective, Atmospheric Chemistry and Physics, 13, 7053-7074, 10.5194/acp-13-7053-2013, 2013.

Zhang, W., Zhu, T., Yang, W., Bai, Z., Sun, Y. L., Xu, Y., Yin, B., and Zhao, X.: Airborne measurements of gas and particle pollutants during CAREBeijing-2008, Atmospheric Chemistry and Physics, 14, 301-316, 10.5194/acp-14-301-2014, 2014.

Zhang, X. P., and Cheng, X. M.: Energy consumption, carbon emissions, and economic growth in China, Ecological Economics, 68, 2706-2712, 10.1016/j.ecolecon.2009.05.011, 2009.

Zhang, X. Y., Wang, Y. Q., Niu, T., Zhang, X. C., Gong, S. L., Zhang, Y. M., and Sun, J. Y.: Atmospheric aerosol compositions in China: spatial/temporal variability, chemical signature, regional haze distribution and comparisons with global aerosols, Atmospheric Chemistry and Physics, 12, 779-799, 10.5194/acp-12-779-2012, 2012.

Zhao, B., Wang, S. X., Liu, H., Xu, J. Y., Fu, K., Klimont, Z., Hao, J. M., He, K. B., Cofala, J., and Amann, M.: NOx emissions in China: historical trends and future perspectives, Atmospheric Chemistry and Physics, 13, 9869-9897, 10.5194/acp-13-9869-2013, 2013a.

Zhao, P. S., Dong, F., He, D., Zhao, X. J., Zhang, X. L., Zhang, W. Z., Yao, Q., and Liu, H. Y.: Characteristics of concentrations and chemical compositions for PM2.5 in the region of Beijing, Tianjin, and Hebei, China, Atmospheric Chemistry and Physics, 13, 4631-4644, 10.5194/acp-13-4631-2013, 2013b.

Zhao, Y., Zhang, J., and Nielsen, C. P.: The effects of recent control policies on trends in emissions of anthropogenic atmospheric pollutants and CO2 in China, Atmospheric Chemistry and Physics, 13, 487-508, 10.5194/acp-13-487-2013, 2013c.

Zhao, Y., Mao, P., Zhou, Y., Yang, Y., Zhang, J., Wang, S., Dong, Y., Xie, F., Yu, Y., and Li, W.: Improved provincial emission inventory and speciation profiles of anthropogenic non-methane volatile organic compounds: a case study for Jiangsu, China, Atmos. Chem. Phys., 17, 7733-7756, 10.5194/acp-17-7733-2017, 2017.

Zheng, B., Chevallier, F., Ciais, P., Yin, Y., Deeter, M. N., Worden, H. M., Wang, Y. L., Zhang, Q., and He, K. B.: Rapid decline in carbon monoxide emissions and export from East Asia between years 2005 and 2016, Environ. Res. Lett., 13, 044007, 10.1088/1748-9326/aab2b3, 2018.

Zhu, Y., Zhang, J., Wang, J., Chen, W., Han, Y., Ye, C., Li, Y., Liu, J., Zeng, L., Wu, Y., Wang, X., Wang, W., Chen, J., and Zhu, T.: Distribution and sources of air pollutants in the North China Plain based on on-road mobile measurements, Atmos. Chem. Phys., 16, 12551-12565, 10.5194/acp-16-12551-2016, 2016.

Tables and Figures

Table 1. List of CMAQ simulations with adjusted emissions based on satellite observations. Anthropogenic CO, NO_x, and VOCs emissions were adjusted using MOPITT CO, OMI NO_2, and OMI HCHO observations.

Run NO.	Experiment Name	Bio. VOCs	Anthro. CO	Anthro. NO_x	Anthro. VOCs
1	CMAQ_baseline	BEIS	EDGAR	EDGAR	EDGAR
2	CMAQ_noBEIS	N/A	EDGAR	EDGAR	EDGAR
3	CMAQ_CO	BEIS	Adjusted	EDGAR	EDGAR
4	CMAQ_NO_x	BEIS	EDGAR	Adjusted	EDGAR
5	CMAQ_VOCs	BEIS	EDGAR	EDGAR	Adjusted
6	CMAQ_All	BEIS	Adjusted	Adjusted	Adjusted

Table 2. Statistics of CMAQ performance of six sensitivity experiments compared with ARIAs aircraft measurements over the NCP.

No.	Name	Mean Diff	Slope	Stdev	Corr. R	NMB	NME	RMSE	Mean Ratio
		ppbv	Unitless	ppbv	Unitless	%	%	ppbv	Unitless
O_3									
1	CMAQ_Baseline	-21.35	0.56	13.25	0.37	-25.14	25.86	25.10	0.75
2	CMAQ_noBEIS	-23.74	0.49	12.85	0.41	-27.94	28.34	26.97	0.72
3	CMAQ_NOx	-19.83	0.59	13.63	0.34	-23.34	24.18	24.03	0.77
4	CMAQ_VOCs	-19.26	0.66	13.66	0.36	-22.67	23.81	23.58	0.77
5	CMAQ_CO	-20.35	0.61	13.52	0.36	-23.96	24.83	24.40	0.76
6	CMAQ_All	-15.18	0.81	14.83	0.33	-17.87	20.33	21.18	0.82
CO									
1	CMAQ_Baseline	-183.56	0.21	165.92	0.23	-60.26	60.26	246.98	0.40
2	CMAQ_noBEIS	-186.34	0.21	165.52	0.25	-61.17	61.17	248.79	0.39
3	CMAQ_NOx	-184.25	0.21	165.76	0.24	-60.48	60.50	247.39	0.40
4	CMAQ_VOCs	-181.89	0.22	166.32	0.22	-59.71	59.78	246.01	0.40
5	CMAQ_CO	-148.55	0.36	167.90	0.22	-48.76	50.32	223.67	0.51
6	CMAQ_All	-104.45	0.52	175.48	0.21	-34.29	45.03	203.60	0.66
NO_2									
1	CMAQ_Baseline	-1.72	0.31	3.09	0.58	-59.91	64.59	3.52	0.40
2	CMAQ_noBEIS	-1.73	0.31	3.09	0.58	-60.47	64.90	3.52	0.40
3	CMAQ_NOx	-1.45	0.38	2.99	0.60	-50.61	61.26	3.31	0.49
4	CMAQ_VOCs	-1.76	0.31	3.10	0.58	-61.60	65.66	3.55	0.38
5	CMAQ_CO	-1.70	0.31	3.09	0.58	-59.28	64.20	3.51	0.41
6	CMAQ_All	-1.47	0.38	3.01	0.59	-51.23	61.62	3.33	0.49
NO									
1	CMAQ_Baseline	-0.25	0.99	0.47	0.68	-32.23	45.4	0.53	0.68
2	CMAQ_noBEIS	-0.24	1.02	0.48	0.68	-31.09	45.66	0.54	0.69
3	CMAQ_NOx	-0.08	1.31	0.59	0.67	-9.75	50.01	0.59	0.90
4	CMAQ_VOCs	-0.30	0.89	0.45	0.68	-38.63	46.58	0.54	0.61
5	CMAQ_CO	-0.26	0.96	0.47	0.68	-33.08	45.26	0.53	0.67
6	CMAQ_All	-0.16	1.13	0.52	0.67	-20.31	45.46	0.54	0.80
NO_y									
1	CMAQ_Baseline	-15.26	0.30	10.15	0.39	-77.58	77.58	18.27	0.22
2	CMAQ_noBEIS	-15.50	0.29	10.15	0.40	-78.81	78.81	18.47	0.21
3	CMAQ_NOx	-14.24	0.37	10.20	0.37	-72.39	72.39	17.46	0.28
4	CMAQ_VOCs	-15.23	0.30	10.16	0.39	-77.42	77.42	18.25	0.23
5	CMAQ_CO	-15.26	0.30	10.15	0.39	-77.56	77.56	18.27	0.22
6	CMAQ_All	-14.21	0.37	10.20	0.37	-72.26	72.26	17.44	0.28

Figure 1. ~~ARIAs flights over the NCP and the WRF-CMAQ domains. Eleven Research Flights (RF) were conducted in May to Mid-June 2016.~~ CMAQ ~~has two~~ domains for the ARIAs campaign (the proximate aircraft campaign area is demonstrated by a red polygon).~~,~~ ~~the~~ The coarse domain (d01, 36 km resolution) covering East Asia and the nested domain (d02, 12 km resolution) focusing on eastern China. ~~a) Summary of flight routes; b) WRF-CMAQ modeling domain (the red dot represents the location of the Xingtai supersite).~~

~~a)~~

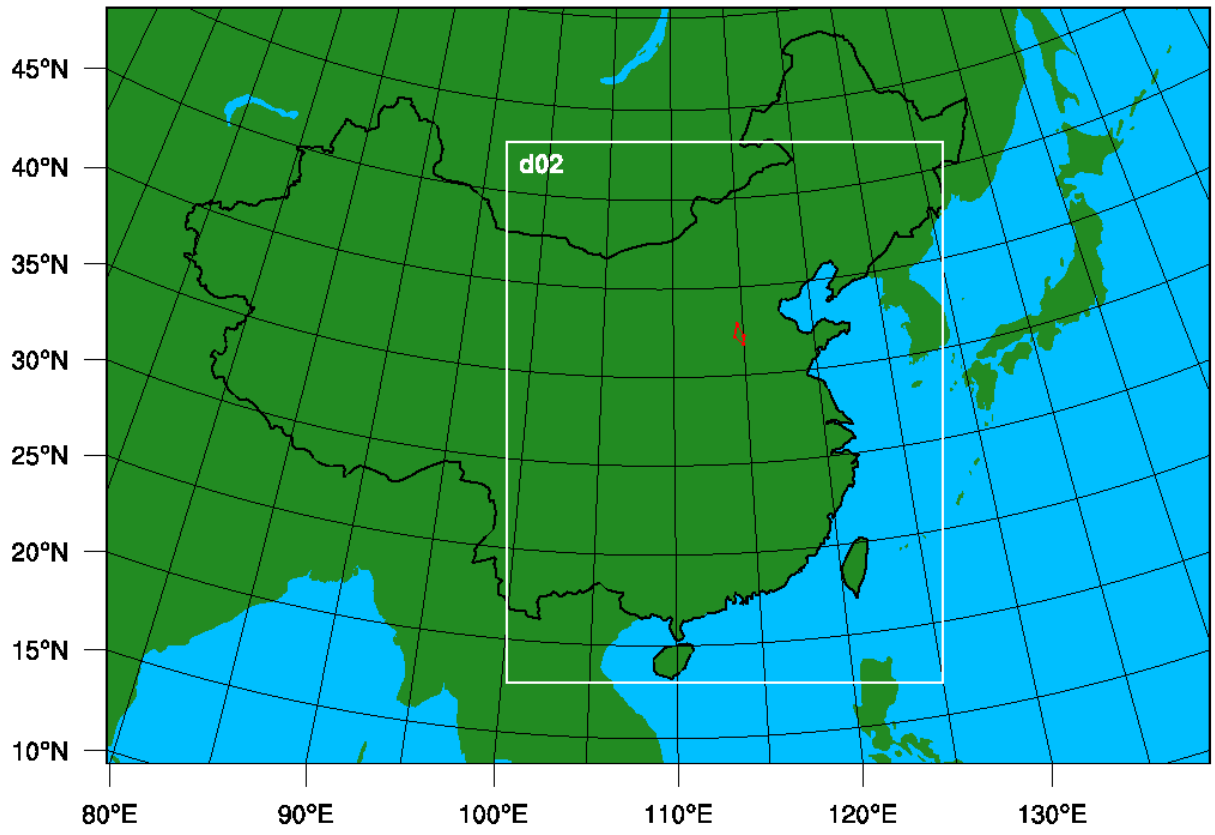

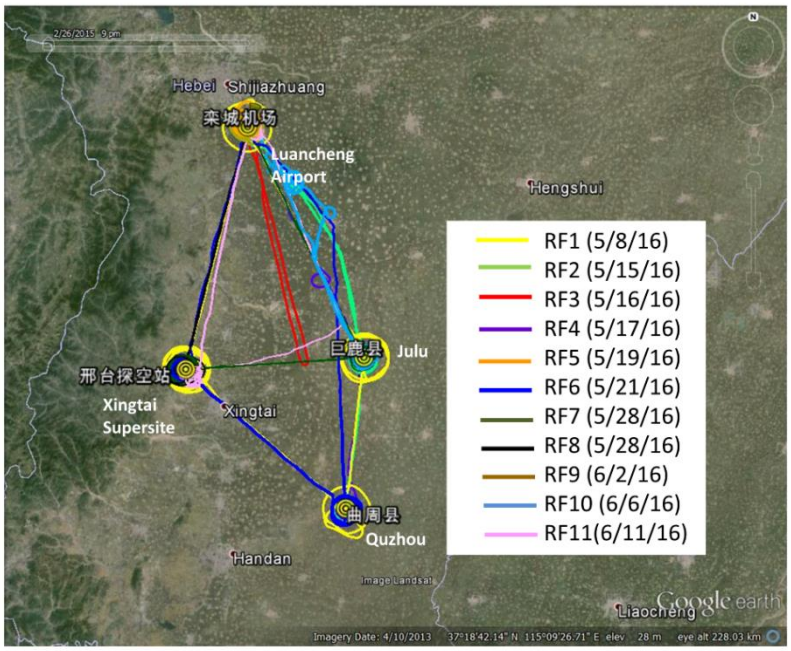
Hebei Shijiazhuang
栾城机场
Luancheng
Airport
Hengshui
RF1 (5/8/16)
RF2 (5/15/16)
RF3 (5/16/16)
RF4 (5/17/16)
RF5 (5/19/16)
RF6 (5/21/16)
RF7 (5/28/16)
RF8 (5/28/16)
RF9 (6/2/16)
RF10 (6/6/16)
RF11(6/11/16)
巨鹿县
Julu
邢台探空站
Xingtai
Supersite
Xingtai
曲周县
Quzhou
Handan
Liaocheng
Google earth

~~b)~~

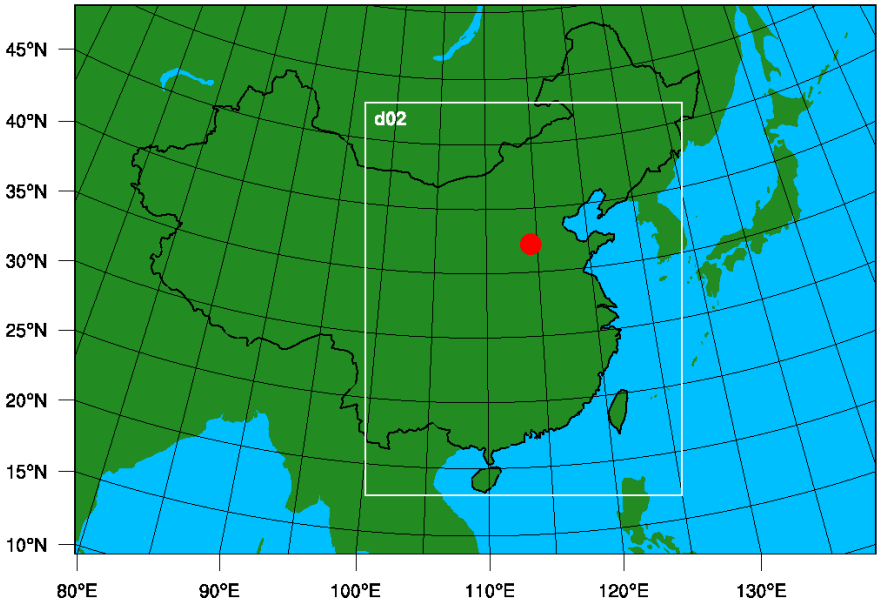
45°N
40°N
35°N
30°N
25°N
20°N
15°N
10°N
80°E
90°E
100°E
110°E
120°E
130°E
d02

Figure 2. Summary of air pollutant concentrations in the NCP observed by Y12 aircraft. a) O_3, b) NO_2, c) CO, and d) CO_2.

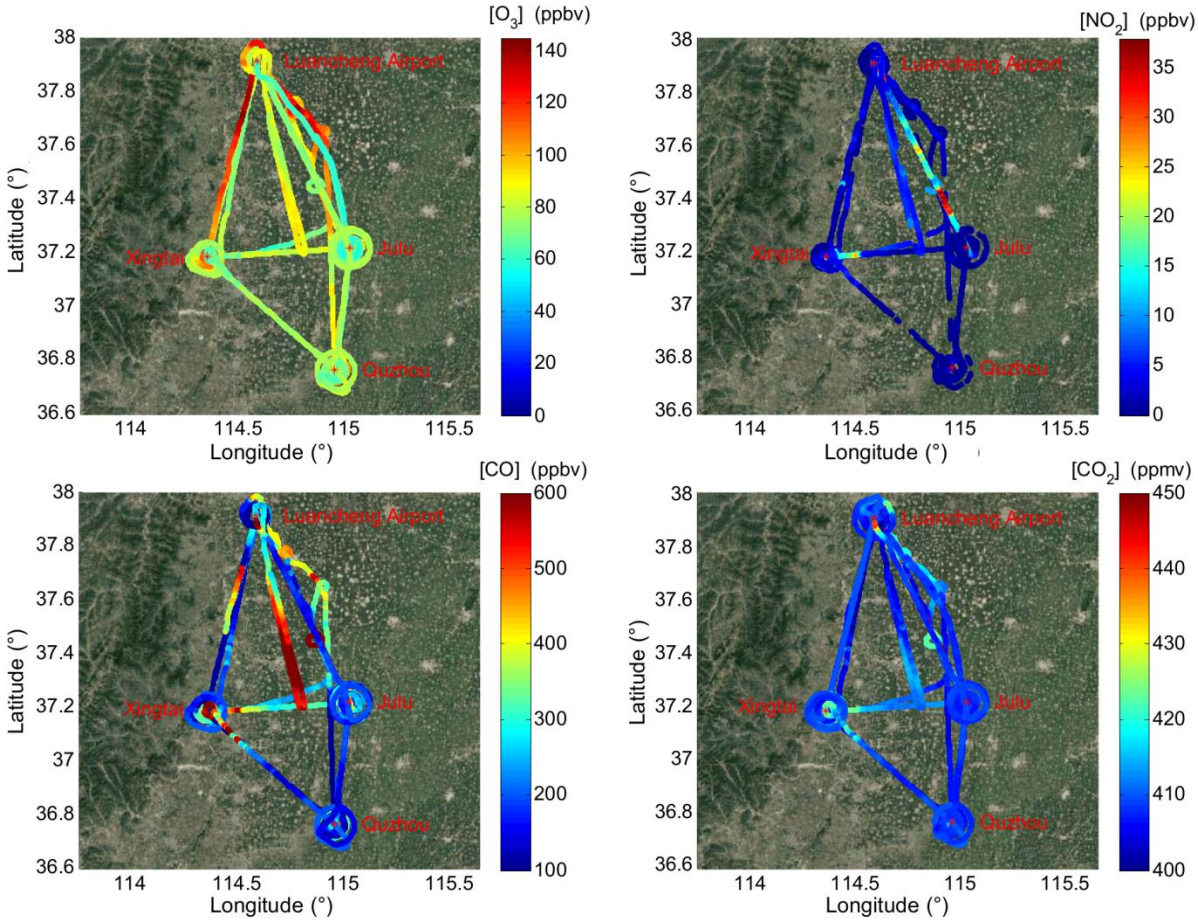

Figure 3. Vertical profiles of air pollutants over four locations in the NCP. a) Xingtai (XT), b) Luancheng (LC), c) Julu (JL), and d) Quzhou (QZ). Red lines show the mean profiles.

a)

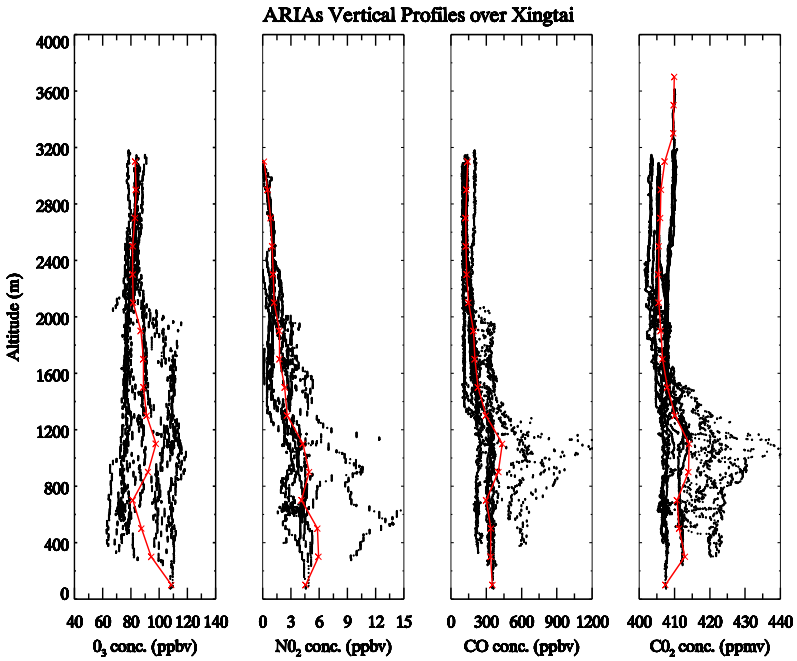

b)

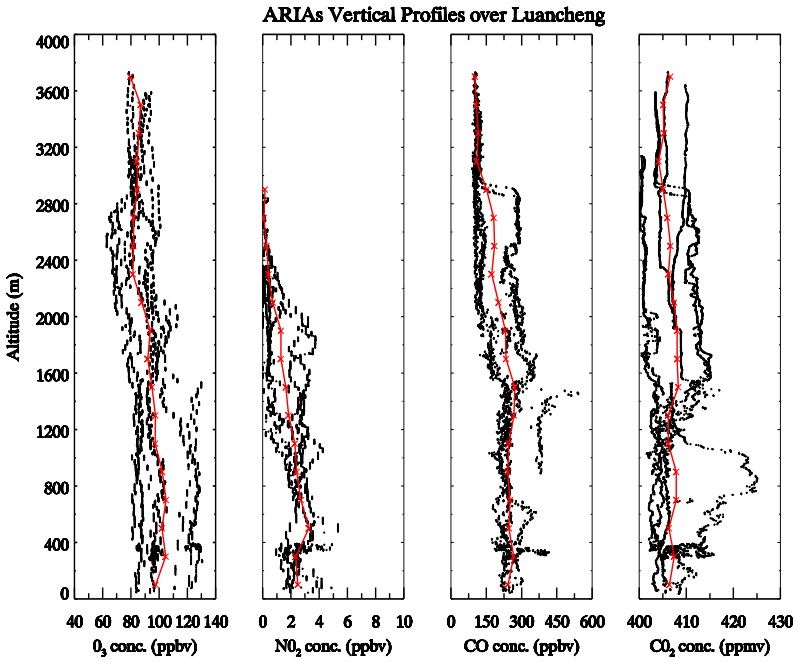

1020 c)

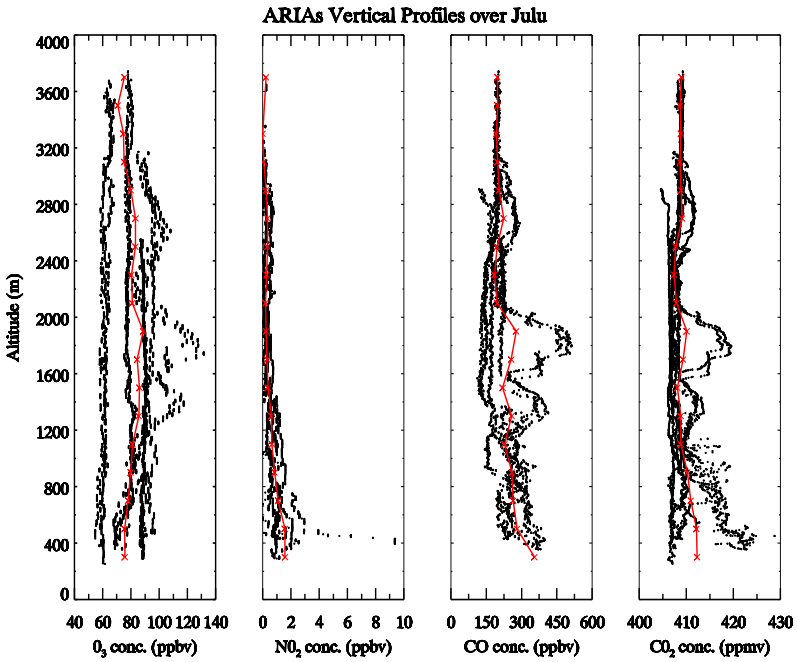

1021
1022 d)

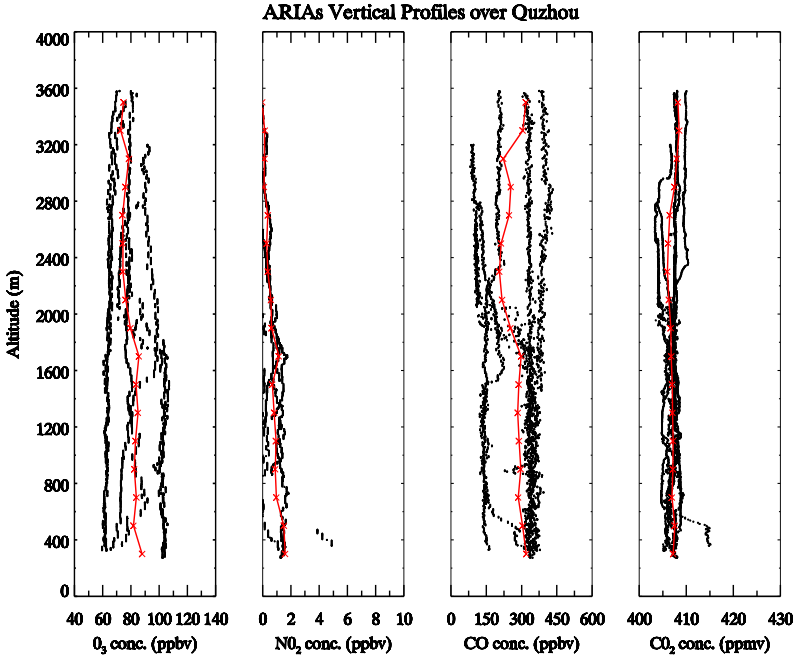

1023

Figure 4. Comparison of 10-min averaged aircraft data and CMAQ simulations from 11 ARIAs research flights. a) O_3, b) CO, c) NO, and d) NO_2. Black line shows the 1:1 ratio; red line stands for the linear regression fitting line. M_Diff: mean difference; R: correlation; NMB: normalized mean bias; NME: normalized mean error; RMSE: root-mean square error; M_Ratio: mean ratio.

a)

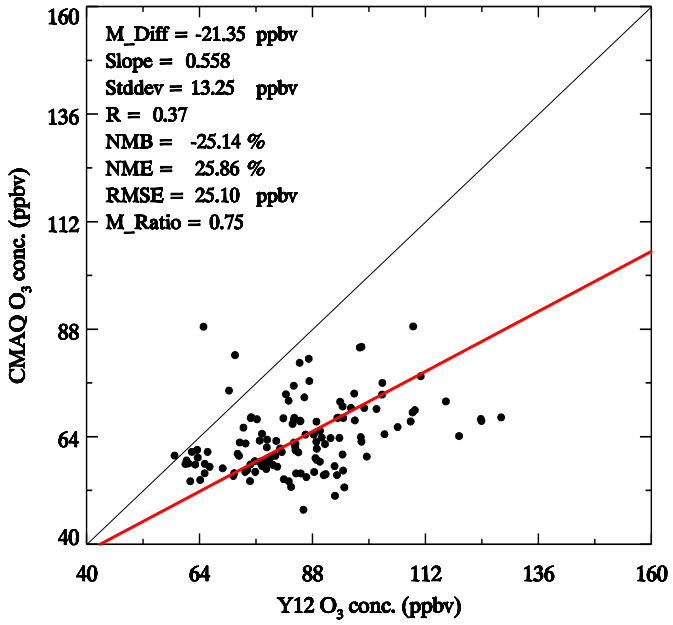

b)

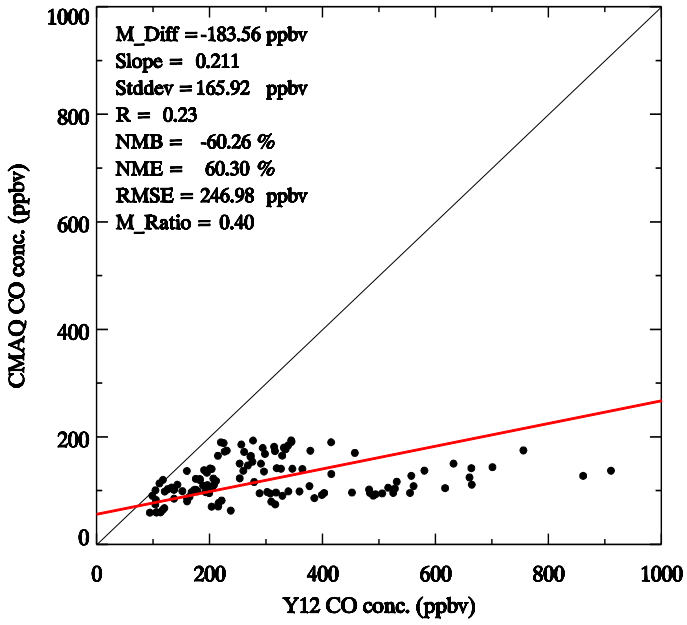

c)

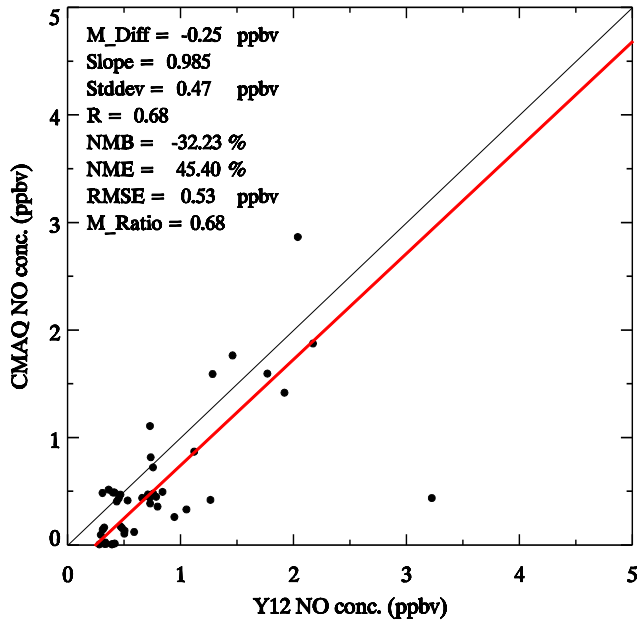
M_Diff = -0.25 ppbv
Slope = 0.985
Stddev = 0.47 ppbv
R = 0.68
NMB = -32.23 %
NME = 45.40 %
RMSE = 0.53 ppbv
M_Ratio = 0.68
CMAQ NO conc. (ppbv)
Y12 NO conc. (ppbv)
0
1
2
3
4
5

d)

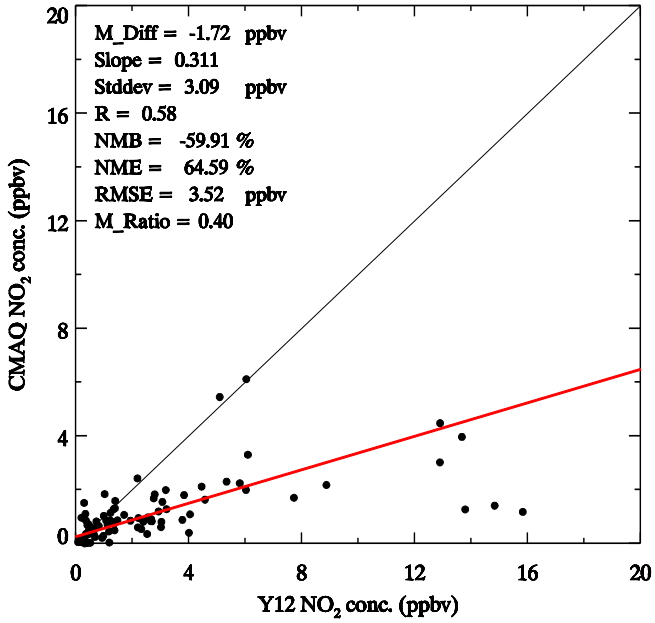
M_Diff = -1.72 ppbv
Slope = 0.311
Stddev = 3.09 ppbv
R = 0.58
NMB = -59.91 %
NME = 64.59 %
RMSE = 3.52 ppbv
M_Ratio = 0.40
CMAQ NO2 conc. (ppbv)
Y12 NO2 conc. (ppbv)
0
4
8
12
16
20

Figure 5. Comparison of total VOCs concentrations from WAS samples and CMAQ simulations. Values are in unit of parts per billion Carbon (ppbC). Black line shows the 1:1 ratio; red line stands for the linear regression fitting line. M_Diff: mean difference; R: correlation; NMB: normalized mean bias; NME: normalized mean error; RMSE: root-mean square error; M_Ratio: mean ratio.

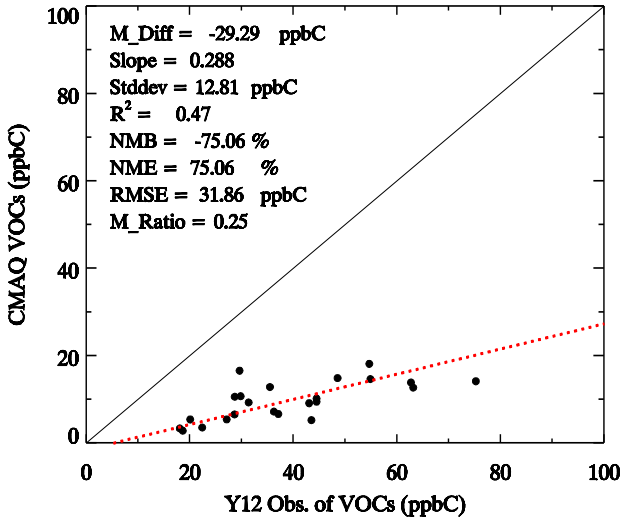

Figure 6. Comparison of emission enhancements (EEs) from the ARIAs campaign and emission factors (EFs) from the EDGAR emission inventory. a) $\Delta CO/\Delta CO_2$, b) $\Delta NO_x/\Delta CO_2$, c) $\Delta NO_x/\Delta CO$. Blue histogram shows the distribution of EEs observed by the Y12 aircraft; red line shows the ratio calculated ~~using~~through ~~–~~ averaging EFs from 4 sectors of the EDGAR anthropogenic emissions inventory.

a)

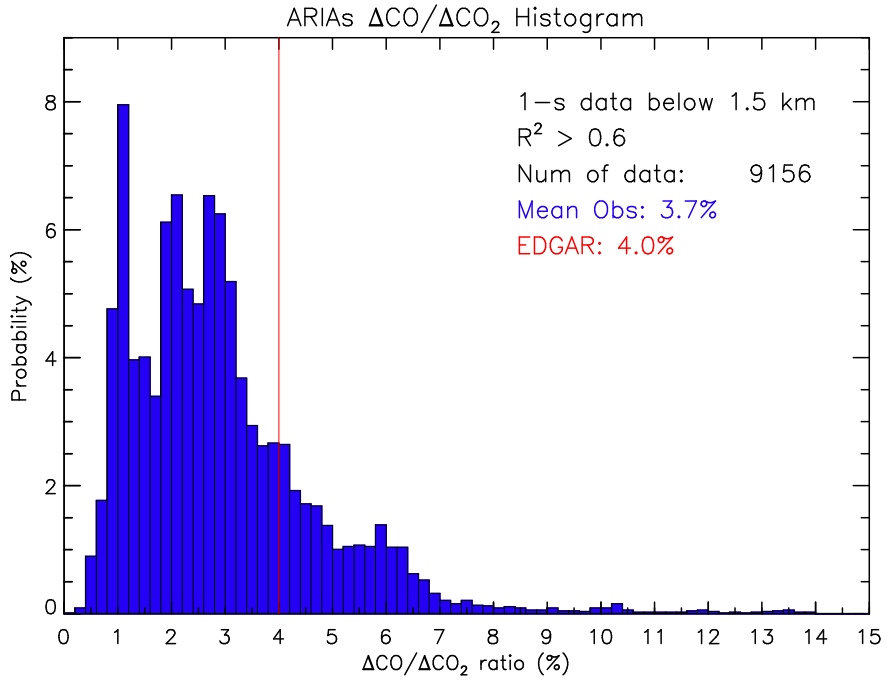

b)

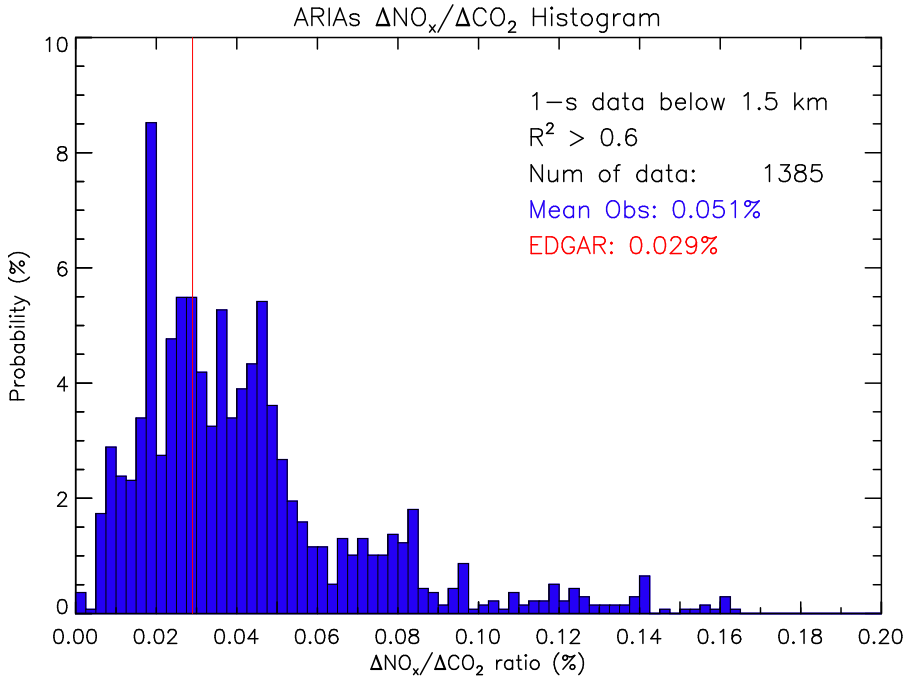

1052 c)

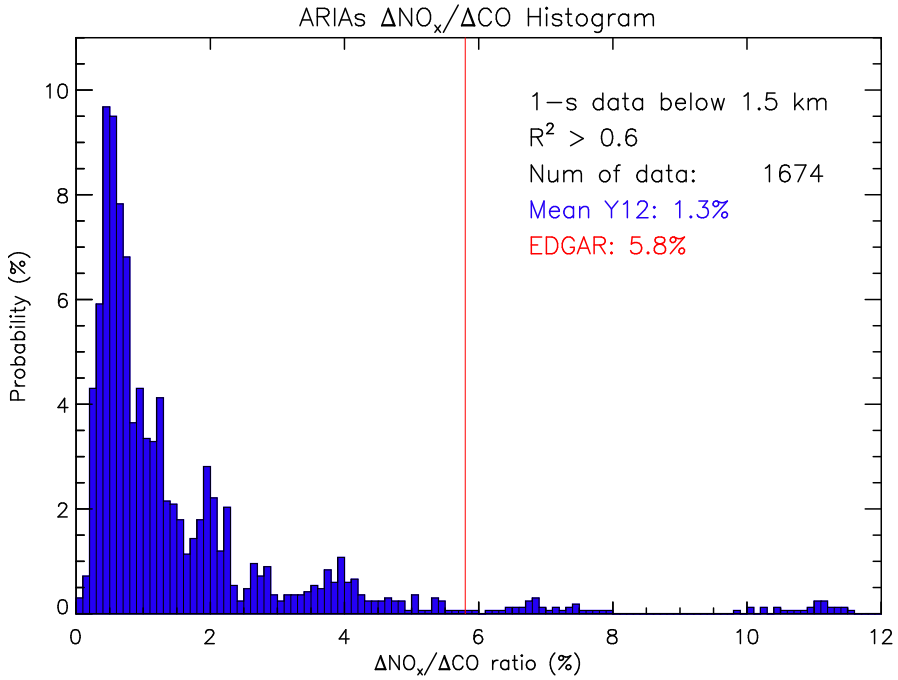
ARIAs ΔNOx/ΔCO Histogram
1−s data below 1.5 km
R2 > 0.6
Num of data: 1674
Mean Y12: 1.3%
EDGAR: 5.8%
Probability (%)
ΔNOx/ΔCO ratio (%)
0
2
4
6
8
10
12

1053

Figure 7. Comparison of air pollutants from satellite observations and CMAQ simulations. a) OMI NO_2 column (left) and the difference between OMI and CMAQ (right), Unit: Dobson Unit (1 DU = 2.69 × 10^{20} molecules/cm^2); b) OMI HCHO column (left) and the difference between OMI and CMAQ (right), Unit: DU; c) MOPITT near surface CO (left) and the difference between MOPITT and CMAQ (right), Unit: ~~(~~ppbv~~)~~. Red star in Fig. 7a stands for the proximate location of aircraft campaign.

a)

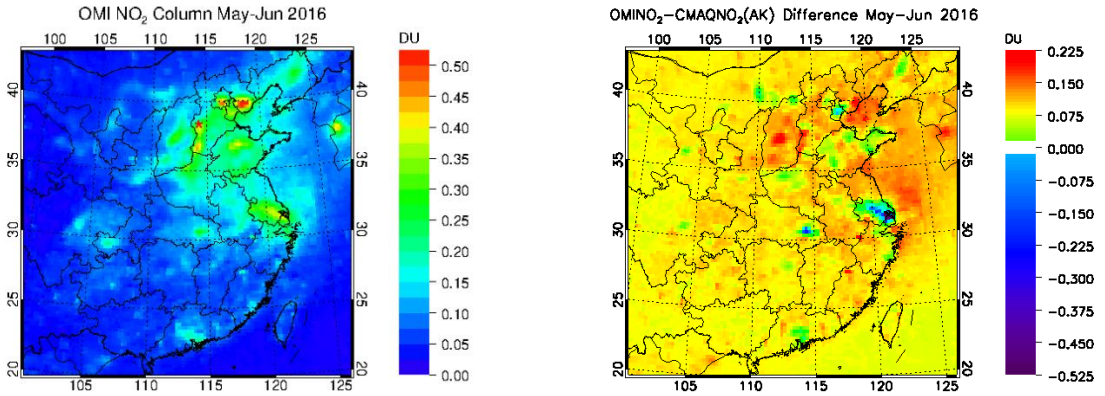

b)

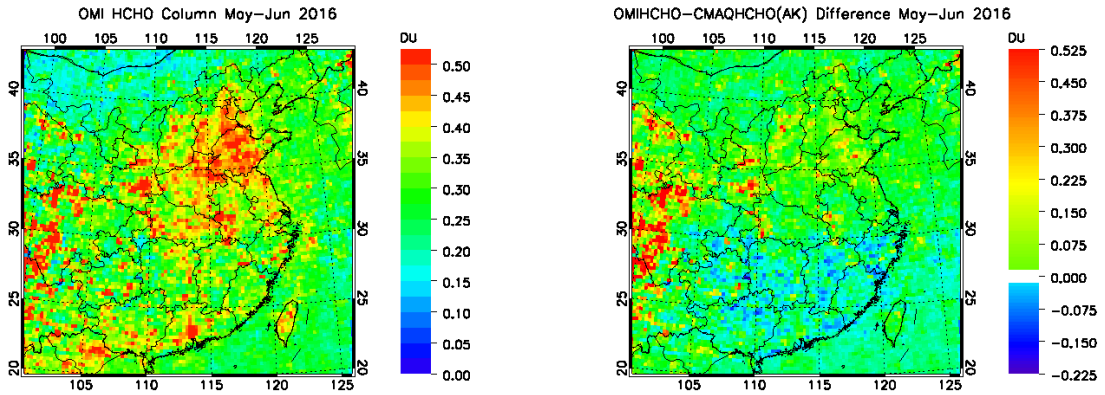

c)

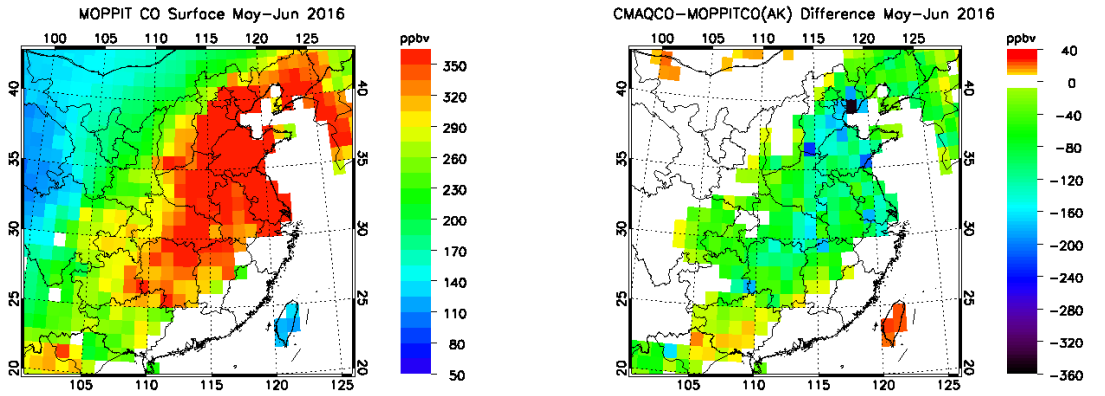

Figure 8. Comparison of OMI NO_2 and CMAQ NO_2 columns averaged in May and June 2016. a) Scatter plot of NO_2 columns over eastern China; b) Scatter plot of NO_2 columns over the campaign area (error bars were calculated as the standard deviation of daily OMI products and daily CMAQ simulations during the 2-month campaign).

a)

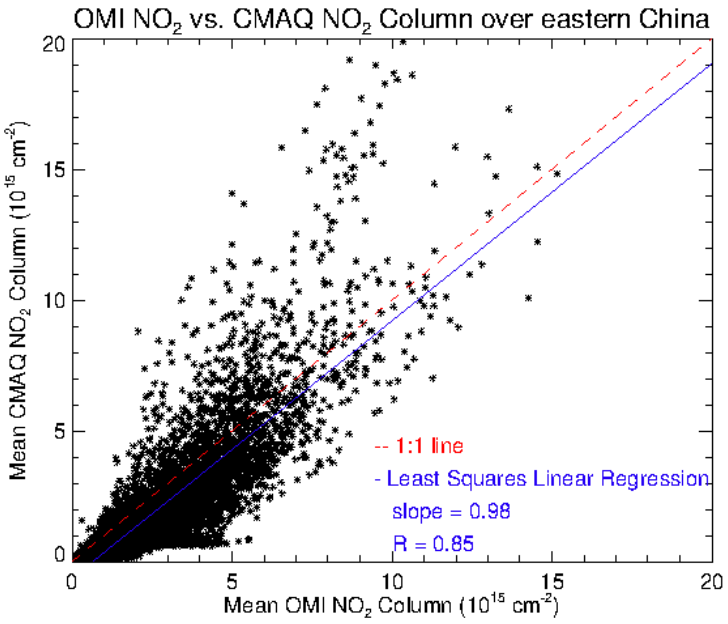

b)

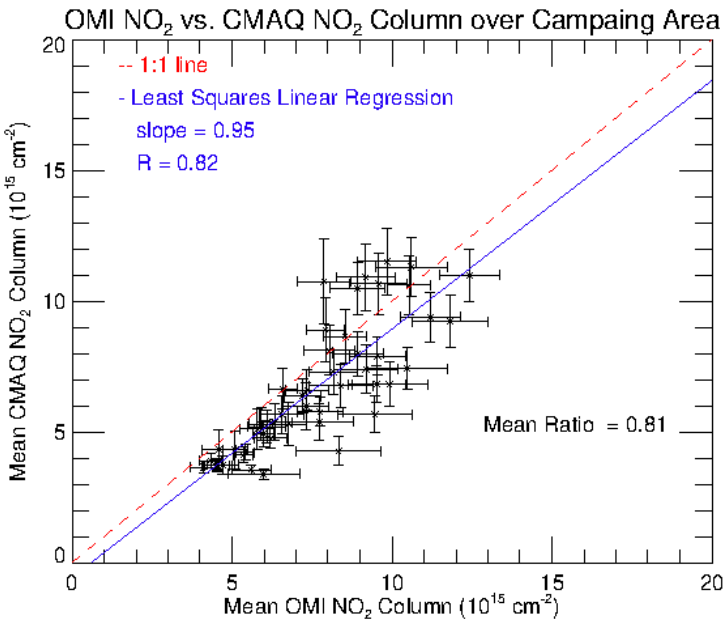

Figure 8. Ratios of column contents of the baseline CMAQ simulations and satellite observations. a) CMAQ/OMI NO_2; b) CMAQ/OMI HCHO; c) CMAQ/MOPITT CO.

a)

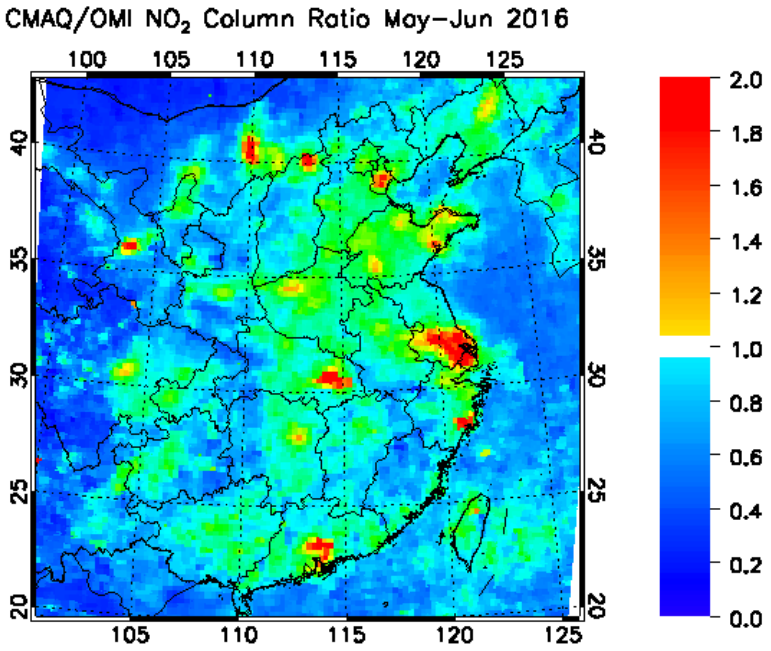

b)

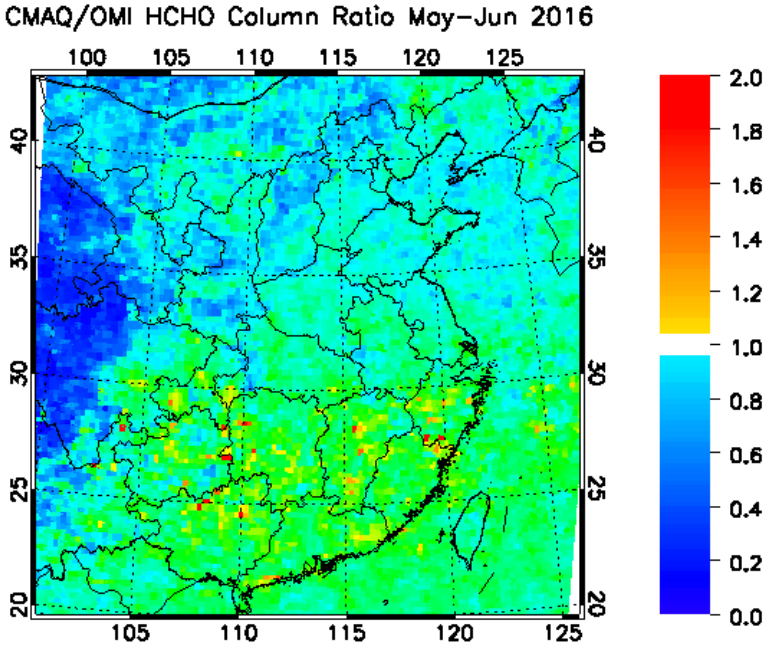

~~c)~~

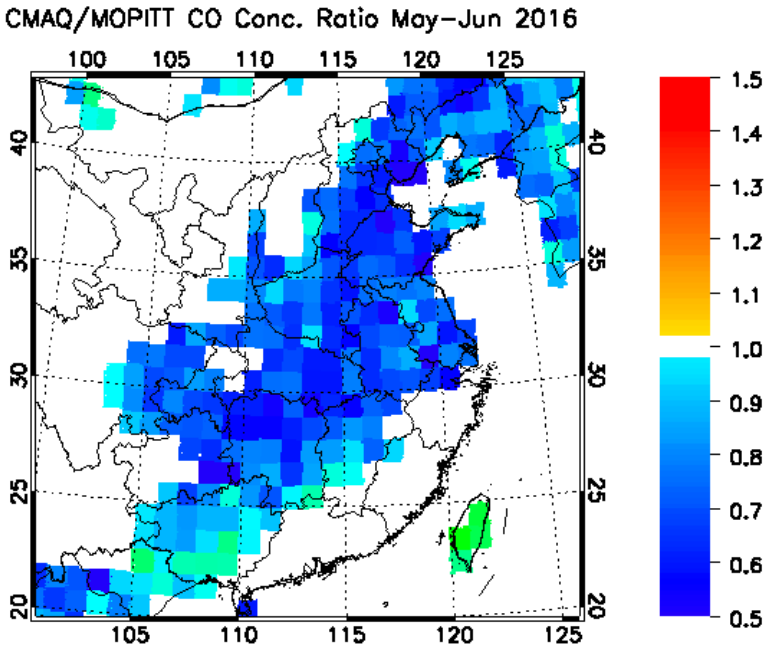
CMAQ/MOPITT CO Conc. Ratio May–Jun 2016
100
105
110
115
120
125
40
35
30
25
20
1.5
1.4
1.3
1.2
1.1
1.0
0.9
0.8
0.7
0.6
0.5

Figure 9. Column $HCHO/NO_2$ ratios over East Asia in spring 2016. a) Ratio derived from collocated OMI HCHO and NO_2 observation; b) Ratio calculated from CMAQ HCHO and NO_2 simulations with OMI quality information and averaging kernel (AK).

a)

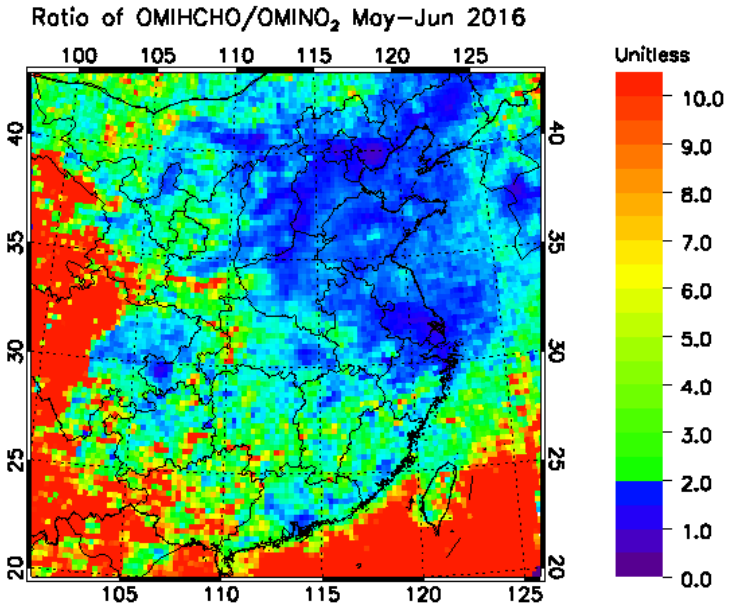

b)

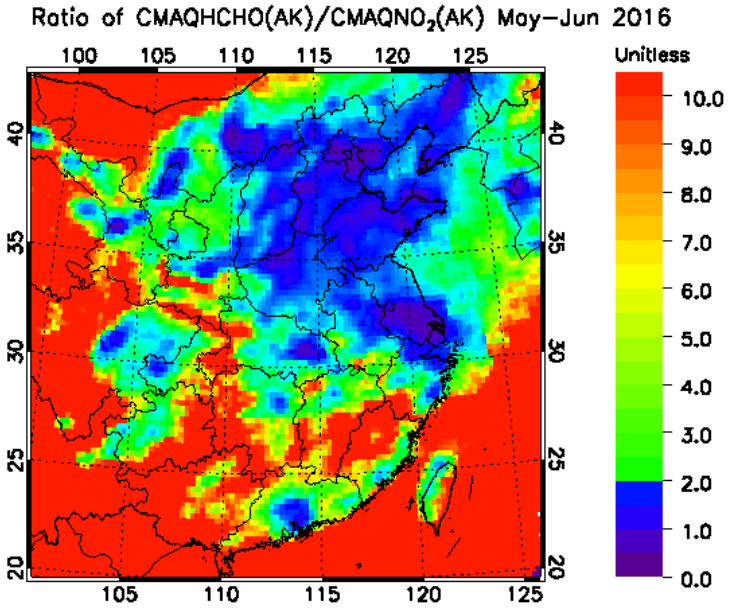

Figure 10. Comparison of surface hourly observations of air pollutants and CMAQ simulations at the Xingtai supersite from May to mid-June 2016. a) O_3, b) CO, c) NO_2^*, d) NO_x, and e) HCHO. *Surface NO_2 is inferred as NO_x-NO from surface observations.

a)

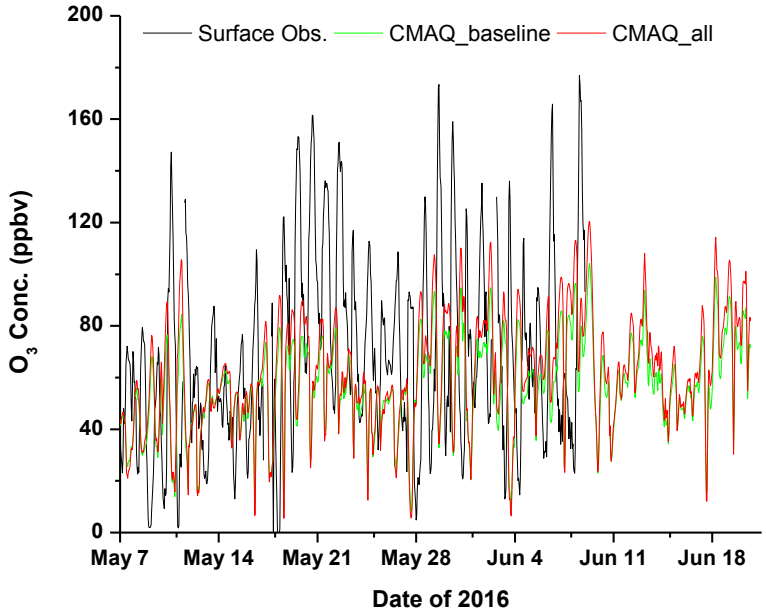

b)

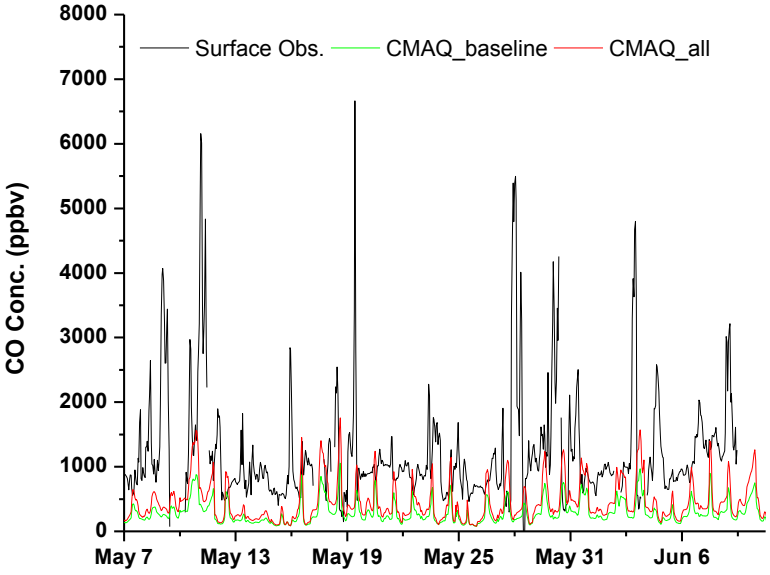

c)

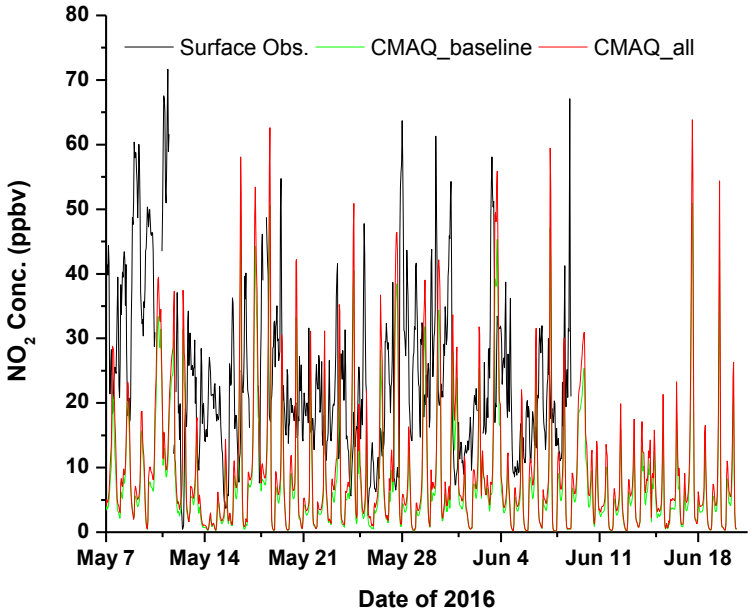
Surface Obs.
CMAQ_baseline
CMAQ_all
NO2 Conc. (ppbv)
0
10
20
30
40
50
60
70
80
May 7
May 14
May 21
May 28
Jun 4
Jun 11
Jun 18
Date of 2016

d)

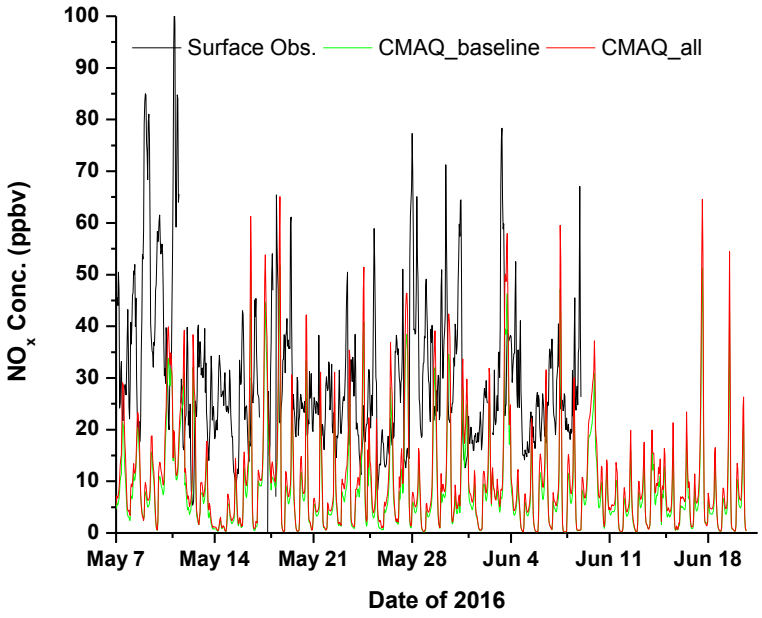
Surface Obs.
CMAQ_baseline
CMAQ_all
NOx Conc. (ppbv)
0
10
20
30
40
50
60
70
80
90
100
May 7
May 14
May 21
May 28
Jun 4
Jun 11
Jun 18
Date of 2016

1102 e)

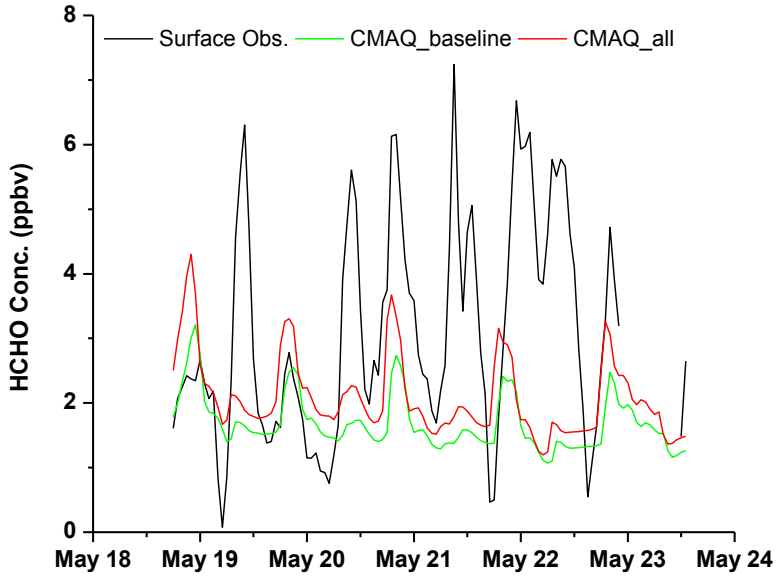
Surface Obs.
CMAQ_baseline
CMAQ_all
HCHO Conc. (ppbv)
0
2
4
6
8
May 18
May 19
May 20
May 21
May 22
May 23
May 24

1103

Figure 11. A case study comparing aircraft observations and the CMAQ_All case results on June 11, 2016. Background: CMAQ simulations. Overlay: 1 min Y12 measurements. a) O_3, b) CO, c) NO_2, d) NO, and e) NO_y.

a)

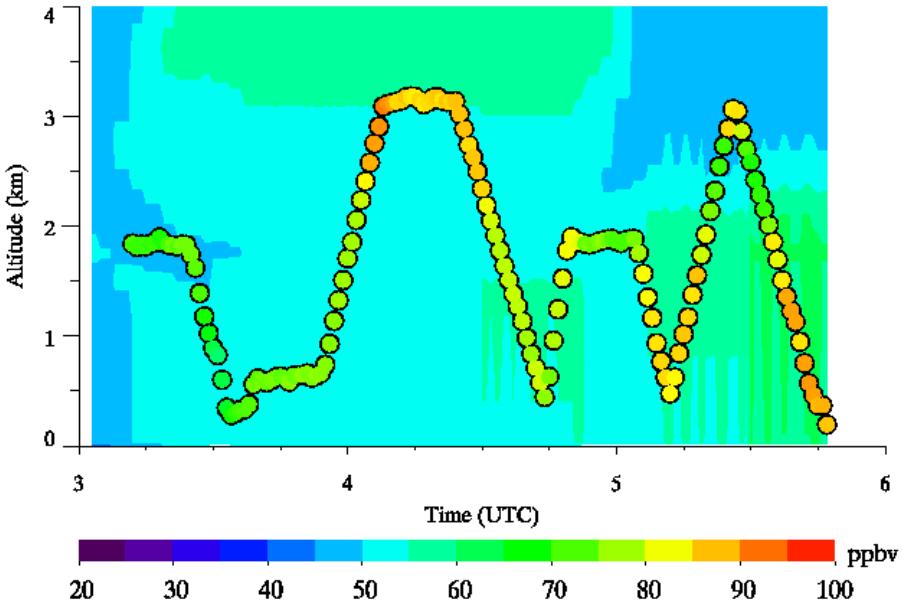

b)

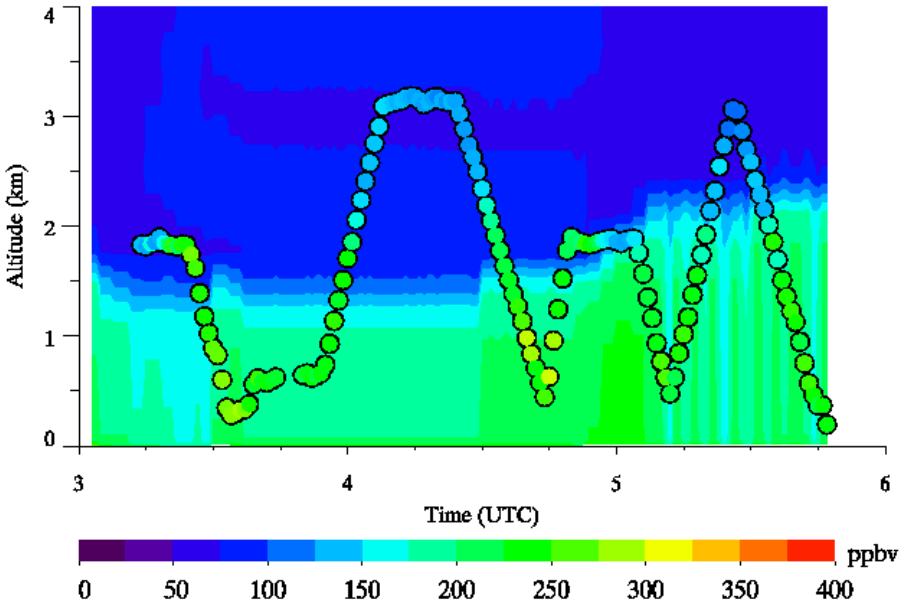

1112 c)

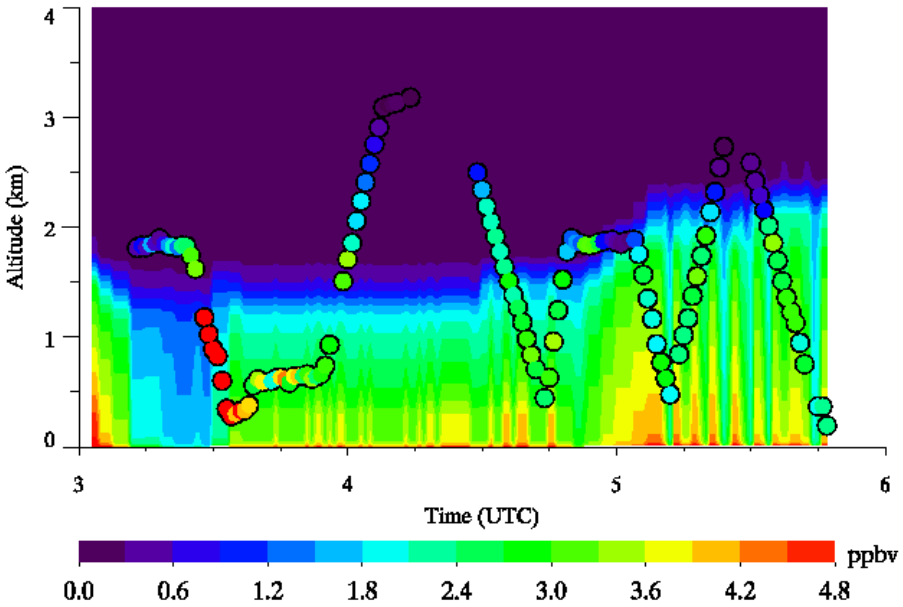

1113
1114
1115 d)

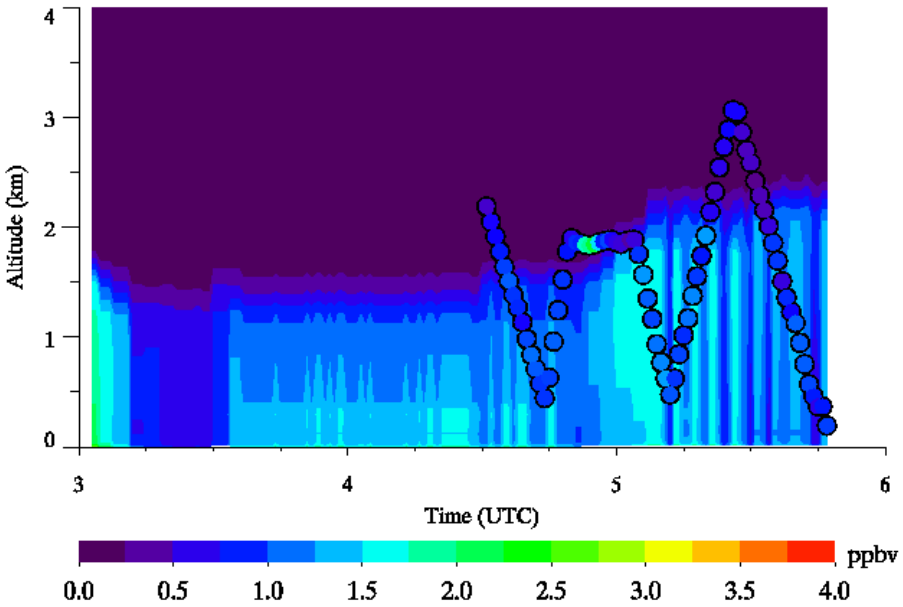

1116
1117

1118 e)

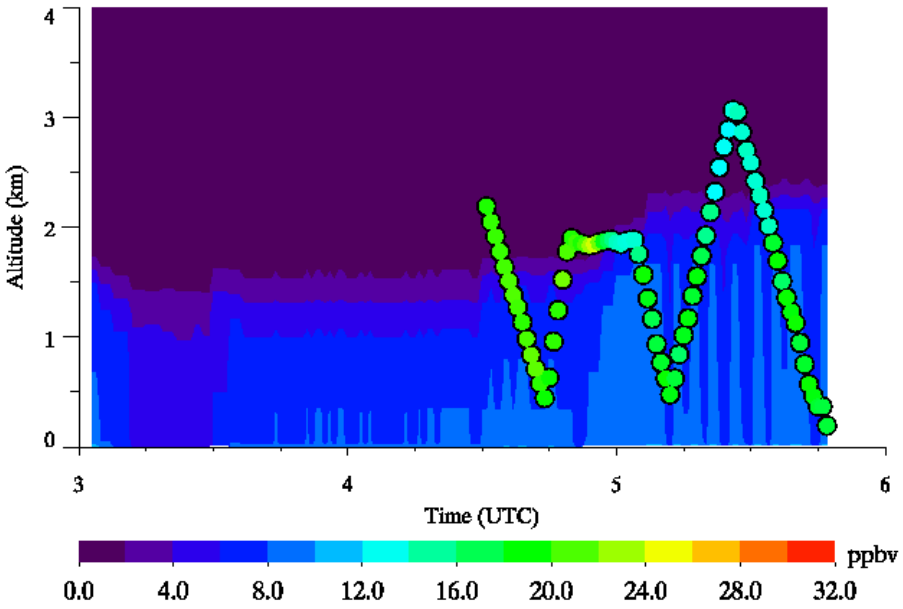
Altitude (km)
0
1
2
3
4
3
4
5
6
Time (UTC)
ppbv
0.0
4.0
8.0
12.0
16.0
20.0
24.0
28.0
32.0

1119